Calmodulin-dependent activation and inactivation of anoctamin calcium-gated chloride channels

Kerstin Vocke,[1] Kristin Dauner,[1] Anne Hahn,[1] Anne Ulbrich,[1] Jana Broecker,[2] Sandro Keller,[2] Stephan Frings,[1] and Frank Möhrlen[1]

[1]Department of Molecular Physiology, Centre for Organismal Studies, Heidelberg University, 69120 Heidelberg, Germany
[2]Molecular Biophysics, University of Kaiserslautern, 67663 Kaiserslautern, Germany

Calcium-dependent chloride channels serve critical functions in diverse biological systems. Driven by cellular calcium signals, the channels codetermine excitatory processes and promote solute transport. The anoctamin (ANO) family of membrane proteins encodes three calcium-activated chloride channels, named ANO 1 (also TMEM16A), ANO 2 (also TMEM16B), and ANO 6 (also TMEM16F). Here we examined how ANO 1 and ANO 2 interact with Ca^{2+}/calmodulin using nonstationary current analysis during channel activation. We identified a putative calmodulin-binding domain in the N-terminal region of the channel proteins that is involved in channel activation. Binding studies with peptides indicated that this domain, a regulatory calmodulin-binding motif (RCBM), provides two distinct modes of interaction with Ca^{2+}/calmodulin, one at submicromolar Ca^{2+} concentrations and one in the micromolar Ca^{2+} range. Functional, structural, and pharmacological data support the concept that calmodulin serves as a calcium sensor that is stably associated with the RCBM domain and regulates the activation of ANO 1 and ANO 2 channels. Moreover, the predominant splice variant of ANO 2 in the brain exhibits Ca^{2+}/calmodulin-dependent inactivation, a loss of channel activity within 30 s. This property may curtail ANO 2 activity during persistent Ca^{2+} signals in neurons. Mutagenesis data indicated that the RCBM domain is also involved in ANO 2 inactivation, and that inactivation is suppressed in the retinal ANO 2 splice variant. These results advance the understanding of Ca^{2+} regulation in anoctamin Cl^- channels and its significance for the physiological function that anoctamin channels subserve in neurons and other cell types.

The Journal of General Physiology

INTRODUCTION

Ca^{2+}-dependent Cl^- currents contribute to a large variety of regulatory processes, including secretory activities in various epithelia, blood pressure control in vascular smooth muscle, and the regulation of neuronal activity (Hartzell et al., 2005; Berg et al., 2012; Huang et al., 2012a). In general, these channels provide a versatile relay between Ca^{2+} signaling and physiological response. Molecular studies of Ca^{2+}-activated Cl^- channels became possible after the discovery that the anoctamin (TMEM16) gene family contains three genes encoding for the Ca^{2+}-activated Cl^- channels anoctamin 1 (ANO 1, also known as TMEM16A; Caputo et al., 2008; Schroeder et al., 2008; Yang et al., 2008), ANO 2 (also known as TMEM16B; Schroeder et al., 2008), and ANO 6 (also known as TMEM16F; Martins et al., 2011). Meanwhile, ANO 1 and ANO 2 channels have been functionally examined to some extent in various cell types, and these studies have provided robust evidence for key roles of ANO channels in the respective cell function (Berg et al., 2012; Huang et al., 2012a). The differential expression of ANO 1 and ANO 2 in individual cell types is of particular interest. ANO 1 displays widespread expression in secretory epithelia, smooth muscle cells, and various other tissues (Huang et al., 2009, 2012b; Schreiber et al., 2010; Dauner et al., 2012). In the nervous system, only two types of peripheral sensory neurons have, so far, been reported to express ANO 1 (Yang et al., 2008; Liu et al., 2010; Cho et al., 2012; Dibattista et al., 2012). In contrast, ANO 2 channels appear to be exclusively expressed in neurons (Pifferi et al., 2009; Stephan et al., 2009; Stöhr et al., 2009; Hengl et al., 2010; Rasche et al., 2010; Huang et al., 2012c; Dauner et al., 2013; Ponissery Saidu et al., 2013). The properties that make ANO 2 channels particularly suitable for neuronal function are only partly understood. One important difference between the two channels appears to be that the Ca^{2+} sensitivity of ANO 2 is ~10-fold lower than in ANO 1. ANO 2 channels need Ca^{2+} concentrations >1 µM for opening (Pifferi et al., 2009; Stephan et al., 2009),

Kerstin Vocke and Kristin Dauner contributed equally to this paper.
Correspondence to Frank Möhrlen: moehrlen@uni-hd.de

Abbreviations used in this paper: aa, amino acid; ANO, anoctamin; Badan, 6-bromoacetyl-2-dimethylaminonaphthalene; CaM, calmodulin; CAMBD1, CaM-binding domain 1; CD, circular dichroism; CRS, CaM recruitment signaling; EPSP, excitatory postsynaptic potential; OE, olfactory epithelium; RCBM, regulatory CaM-binding motif; RT-PCR, reverse transcription polymerase chain reaction; TFP, trifluoperazine; TMR, transmembrane region; wt, wild type.

The Rockefeller University Press $30.00
J. Gen. Physiol. Vol. 142 No. 4 381–404
www.jgp.org/cgi/doi/10.1085/jgp.201311015

whereas ANO 1 channels are activated at 0.1–0.3 µM Ca^{2+}, depending on the splice variant of the channel (Ferrera et al., 2009). Consequently, ANO 1 channels can be constitutively open in an epithelial cell with continuous transport activity. In neurons, however, ANO 2 gating can only be driven by elevated Ca^{2+} levels during signaling activity. Thus, with respect to their Ca^{2+} sensitivity, ANO 2 channels appear to be specifically tailored for processing transient signals.

It is not yet understood how Ca^{2+} opens ANO 1 and ANO 2 channels. Mutagenesis approaches have pinpointed several regions that codetermine the channels' sensitivity to Ca^{2+} and to voltage (Ferrera et al., 2009; Xiao et al., 2011; Cenedese et al., 2012; Yu et al., 2012). However, the nature of the channels' interaction with Ca^{2+} and the mechanism of gating are still not understood satisfactorily. Moreover, biophysical exploration of ANO channels revealed that ANO 1 and ANO 2 channels are subject to various modes of activity modification. Evidence was reported for a reversible Ca^{2+}-dependent inactivation (Reisert et al., 2003; Pifferi et al., 2009) as well as for regulatory effects of calmodulin (CaM) and ATP (Tian et al., 2011). Moreover, the anion selectivity of ANO 1 and ANO 2 channels changes over time in a Ca^{2+}-dependent fashion (Sagheddu, C., A. Boccaccio, and A. Menini. 2011. Abstracts from the XXth Congress of European Chemoreception Research Organization, ECRO-2010, Avignon, France; Jung et al., 2013), and a phosphorylation/dephosphorylation equilibrium appears to be involved in the regulation of these channels in smooth muscle (Angermann et al., 2006; Ayon et al., 2009; Davis et al., 2010). A prominent feature in ANO 1 and ANO 2 is an exponential loss of channel function in inside-out patches (Reisert et al., 2003; Kaneko et al., 2006; Pifferi et al., 2009; Stephan et al., 2009; Ponissery Saidu et al., 2013). This run-down could not be stopped by application of compounds like adenosine triphosphate, the reducing agent dithiothreitol, the signaling compound phosphatidylinositol trisphosphate, CaM, cAMP, or the phosphatase inhibitor sodium vanadate (Pifferi et al., 2009). In one study (Tian et al., 2011), a combination of ATP and CaM induced a partial reversal of the run-down in ANO 1 channel activity after patch excision. Run-down caused a 60–100% loss of channel currents over ∼10 min. The inherent plasticity of ANO function and its instability in isolated patches hampers functional exploration. Most published studies have been performed in the whole-cell configuration with internally perfused cells that express ANO 1 or ANO 2. After Ca^{2+} equilibration between cytosol and pipette solution, voltage pulses were applied, and the resulting currents were analyzed. To obtain data from excised patches despite the run-down problem, researchers usually await a steady-state of the Ca^{2+}-dependent Cl^- current across the patch membrane and analyze this residual current for their experiments. In this way, important insights into Ca^{2+} dependence, voltage dependence, and ion permeation have been obtained (Reisert et al., 2003; Pifferi et al., 2009; Stephan et al., 2009; Xiao et al., 2011; Yu et al., 2012; Li et al., 2013). However, the question of the activation mechanism is still unsolved.

In the present study, we approach the question of ANO channel activation with a different recording method. Using a nonstationary approach that mimics channel activation upon the onset of a cellular Ca^{2+} signal, we leave the channels in contact with cellular constituents that may be important for gating. By restricting analysis to the initial minute of channel activation, a time period when regulatory processes may not yet have become effective, we largely avoid modulatory processes and run-down effects. We could identify a putative CaM-binding domain that is involved in the Ca^{2+}-dependent activation in ANO 1 and ANO 2. Furthermore, we found that two splice forms of the neuron-specific ANO 2 channel display a functional difference that is critical for signal processing: one splice form shows CaM-mediated inactivation, whereas the other doesn't. Our study illustrates that the ANO proteins provide a multifunctional set of Ca^{2+}-activated anion channels and are able to operate at either low or high Ca^{2+} concentration, with either phasic or tonic gating characteristics.

MATERIALS AND METHODS

Molecular cloning of rat ANO 1 and ANO 2

mRNA of rat olfactory epithelium (OE) was isolated using Dynabeads Magnetic Beads (Invitrogen; Life Technologies). cDNA was made by reverse transcription using random hexamer primers (Thermo Fisher Scientific) and SuperScript III Reverse transcription (Invitrogen). The primers used for full-length cloning (Table S2) spanned the entire open reading frame of rat ANO 1 (Hartzell et al., 2009) and ANO 2 (Stephan et al., 2009). An NheI site was introduced at the 5′ end and a BamHI (ANO 1) or SmaI (ANO 2) site at the 3′ end of the fragments for fusing YFP to the C terminus of ANO 1 and ANO 2 in the expression vector pEYFP-N1 (Takara Bio Inc.). The resulting constructs were verified by sequencing. Rat ANO 1 protein sequence from OE corresponds to database entry NP_001101034 starting with amino acid (aa) position M59. In addition, V528 to C531 is replaced by the aa sequence EAVK (5′-GAAGCTGTCAAG-3′) due to an incorrect splicing site prediction in rat. Rat ANO 2 from OE corresponds to XP_003753992 starting with aa position M23. The photoreceptor isoform of mouse ANO 2 in the expression vector pCMV-Sport6 was obtained from the German Science Centre for Genome Research (RZPD; clone identification: IRAVp968H1167D; see also Pifferi et al., 2009).

Site-directed mutagenesis of ANO 1 and ANO 2

Mutagenesis was performed using the QuikChange II XL Site-Directed Mutagenesis kit (Agilent Technologies) according to the manufacturer's instructions, and all constructs were sequenced before use. The following amino acids were targeted for mutagenesis (for primers see Table S2). ANO 1: L323E, W327E, V332E, and Y336E. ANO 2: L309E, W313E, V318E, F322E, and L327E. The following deletions/insertions were made. ANO 1: ΔE470 to K473. ANO 2: insert E456 to Q459 (ERSQ). To produce ANO 1 and ANO 2 chimeras, Eco105I and EcoRI restriction sites were inserted without changing the amino acid sequence (Table S2).

Cloning of CaM mutants

Wild-type (wt) CaM and CaM mutants in the expression vector pcDNA3 were provided by D.T. Yue (Johns Hopkins University School of Medicine, Baltimore, MA). In these mutants the EF hand Ca^{2+}-binding sites in the two binding lobes were disabled by D→A exchanges (for further details, see Kaneko et al., 2006). For the identification of heterologous CaM in transfected cells by patch-clamp analysis, the constructs were tagged at the N-terminal domain with the red fluorescent protein variant mRFP-Q66T (Jach et al., 2006) in pcDNA3.1.

Heterologous expression and electrophysiology

Expression of cloned cDNAs encoding ANO 1, ANO 2, and CaM in HEK 293 cells was performed with MATra-A Reagent (PromoKine) according to the manufacturer's instructions. As a reporter for transfection efficiency and expression (wt and mutants), recombinant fusion genes carrying N- or C-terminal yellow fluorescent protein tags were used. For patch-clamp recording, cells were grown on poly-L-lysine–coated coverslips and transferred to the recording chamber on the stage of an upright microscope (Eclipse; Nikon). All experiments were done in CsCl solution to suppress Ca^{2+}-dependent cation currents, in particular K^+ currents. The bath solution contained (in mM): 150 CsCl, 10 HEPES, and 10 EGTA, pH 7.4 (CsOH). The pipette solutions contained 150 mM Cl^-, 10 mM HEDTA, and 10 mM HEPES, pH 7.0 (CsOH). Cs^+ and Ca^{2+} concentrations were included at a total cation concentration of 150 mM, with Ca^{2+}/HEDTA designed to give the desired free Ca^{2+} concentrations. The exact compositions of all pipette solutions are listed in Table S1. Free Ca^{2+} concentrations were determined with a calcium electrode (KWIKCAL-2, CALBUF-1; World Precision Instruments) as 0.7 µM, 2.0 µM, 2.6 µM, 7.5 µM, and 62 µM. Pipette solutions were frozen in aliquots and used for the entire study. Transfection efficiency was mostly near 1%. Cells were selected for healthy appearance and similar brightness of YFP fluorescence to ensure comparable degrees of protein expression in all cells examined. On-cell gigaseals were established using borosilicate capillaries (outer diameter = 1.5 mm, inner diameter = 0.86 mm) with a resistance of 5–8 MΩ connected to a patch-clamp amplifier (EPC-8; HEKA). After setting the pipette voltage to −70 mV, whole-cell access was achieved by disrupting the membrane patch inside the pipette using negative pressure. The pipette current was continuously monitored after filtering at 10 kHz, digitization (BNC 2120; National Instruments), and sampling at 5 kHz using the Strathclyde Electrophysiology Software WinWCP provided by the University of Strathclyde (Glasgow, Scotland, UK). For variance analysis, current recordings were high-pass filtered at 2–10 Hz and subjected to running-average analysis with time segments of 0.1–1 s to determine the current amplitude (I) and the current variance (σ^2). Variance analysis was based on the assumption that the Ca^{2+}-activated Cl^- channels form a homogenous channel population with one closed and one open state. Under this condition, variance and current are related according to $\sigma^2 = iI - I^2/N$, with i representing the single-channel current and N the number of active channels (Sigworth, 1980). This relation permits monitoring changes in open probability (P_o), as illustrated in the text.

Wheat germ agglutinin cell surface staining

Transfected cells were fixed with 4% paraformaldehyde for 15 min at room temperature. After washing three times with Hank's balanced salt solution (HBSS; in mM: 137 NaCl, 5.4 KCl, 0.3 Na_2HPO_4, 0.4 KH_2PO_4, 4.2 $NaHCO_3$, 1.3 $CaCl_2$, 0.5 $MgCl_2$, 0.6 $MgSO_4$, and 5.6 D-glucose 5, pH 7.5), cells were incubated for 10 min with tetramethyl rhodamine-conjugated wheat germ agglutinin (WGA; 2 µg/ml; Molecular Probes; Life Technologies). Cells were washed twice with HBSS and incubated for 1 min with 0.3 µM 4,6-diamidino-2-phenylindole (DAPI; C-7509; Molecular Probes). After three additional washing steps with HBSS, coverslips were mounted on glass slides using Aqua-Poly/Mount (Polysciences, Inc.). Stainings were analyzed using a spectral imaging confocal laser scanning system (Nikon C1).

Characterization of ANO 2 splice variants

To identify the splice variant of segment *c* (exon 13 in human ANO 1; Ferrera et al., 2009) expressed in the neuronal ANO 2 channels, reverse transcription PCR (RT-PCR) was performed on retina, pineal gland, cortex, hippocampus, cerebellum, brain stem, and olfactory cDNA with primers that overlap rat exon 15 (Table S2). RNA from the rat tissues was extracted using the Magnetic mRNA Isolation kit (No. S1550S; New England Biolabs, Inc.). cDNA was synthesized using 200 ng mRNA, random hexamer primers, and RevertAid Premium (Thermo Fisher Scientific). PCR amplification was performed on 0.2 ng single-stranded cDNA with 2U *Thermus aquaticus* (Taq) DNA polymerase (Axon). Cycling conditions were 94°C for 3 min, 94°C for 30 s, 60°C for 20 s, 72°C for 30 s for 32 cycles, respectively, and 72°C for 8 min. Controls were performed on the cloned olfactory and retinal ANO 2 splice variants (see "Molecular cloning of rat ANO 1 and ANO 2"). The bands were resolved by gel electrophoresis and verified by sequencing.

Immunoprecipitation and CaM-binding assays

For immunoprecipitation experiments, stable cell lines were generated that express YFP/ANO 1 or YFP/ANO 2. This was necessary because the ANO expression efficiency in transient transfections was too low for immunochemistry, with transfection rates near 1%. HEK 293 cells were transfected using the calcium phosphate method, applying 1 µg/µl YFP/ANO 1, YFP/ANO 2 transfection vector to the cells. 48 h after transfection, cells were split and 80 µg/µl G418 antibiotic was added for selection of transfected clones. 7 d later, cell colonies were tested for YFP fluorescence and transferred to 24-well plates. Stably transfected cells were grown on 10-cm plates, and aliquots were stored in liquid nitrogen. For growing the cells on 10-cm dishes, no G418 was added to the medium. Cells were harvested from eight 10-cm plates and resuspended in lysis buffer (in mM: 150 NaCl, 2 $CaCl_2$, 1 $MgCl_2$, and 50 Tris/HCl, pH 7.2, containing 1% Triton X-100 and the protease inhibitor PMSF, diluted 1:100). After 15 min of incubation on a rotator at 4°C, cells were mechanically treated with a pestle, followed by a second incubation time on a rotator at 4°C. The lysate was centrifuged at 12,000 *g* for 30 min at 4°C, and the supernatant was sterile filtrated. A preclearing step with Protein A Sepharose was performed for 25 min at 4°C on a rotator. Afterward, the lysate was centrifuged and the supernatant was incubated with the anti–green fluorescent protein (anti-GFP) antibody (ab290; Abcam) for 4 h at 4°C. Protein A Sepharose was added to the lysate/antibody mixture and incubated at 4°C for 2 h on a rotator. The probe was centrifuged, washed three times with washing buffer (in mM: 150 mM NaCl, 2 $CaCl_2$, 1 $MgCl_2$, and 50 Tris/HCl, pH 7.2, containing 0.25% Triton-X 100 and PMSF, diluted 1:500) and boiled at 70°C in SDS/DTT buffer for 15 min. Proteins were separated by SDS-PAGE on 12.5% gels. One half of the samples were Coomassie-stained and used for mass spectrometry. Mass spectrometry was performed at the ZMBH Core Facility for Mass Spectrometry and Proteomics (Heidelberg University), using a mass spectrometer (ESI-LTQ Orbitrap MS; Thermo Fisher Scientific). Data were analyzed by Scaffold Viewer software version 3.5.1 (Proteome Software). The other half of the protein samples were electrophoretically blotted on PVDF membranes. Membranes were blocked with 5% milk powder (in PBS/1%Triton X-100) for 1 h and then incubated with primary antibodies for at least 4 h. After three washing steps in PBS, the secondary antibody was added and incubated for

1.5 h. Blots were washed again, and chemiluminescence was detected via ECL Western blotting detection reagents (GE Healthcare). Primary antibodies against ANO 1 and ANO 2 were raised in guinea pigs and were previously tested for selectivity (Dauner et al., 2012). Secondary antibodies were αgp peroxidase conjugate and αrb peroxidase conjugate (Sigma-Aldrich).

For peptide-binding assays, regulatory CaM-binding motif (RCBM)-related peptides were synthesized by Peptide Specialty Laboratories. Amino-acid sequences corresponded to the RCBM sequences shown in Fig. 5 C, including the two flanking RK motifs. The sequence of the control peptide, ANO ctrl, was RKLEYEEEASYGVFYKEQPIDEVRK. A 6-bromoacetyl-2-dimethylaminonaphthalene (Badan) tag (Owenius et al., 1999) was linked to each peptide via an additional C-terminal cysteine. Each Badan peptide was dissolved in Ca^{2+} buffer at 3 µM together with 1.5 µM CaM. Steady-state fluorescence was obtained on a spectrofluorimeter (LS50; Perkin-Elmer) in quartz cuvettes (Hellma) in a sample volume of 100 µl. Fluorescence emission spectra were recorded between 400 and 600 nm upon excitation at 387 nm (bandwidth 5–10 nm, scan speed 200 nm/min). CaM mutants CaM1234, CaM12, and CaM34 were expressed and purified as described previously (Ungerer et al., 2011). Wt CaM was purchased from Merck (No. 208690). Ca^{2+} solutions were prepared in 100 mM NaCl, 20 mM HEPES, and 10 mM Ca^{2+} buffer at pH 7.2. Ca^{2+} buffers were EDTA for 0.007–0.2 µM (Patton et al., 2004), EGTA for 0.3–2 µM (Williams and Fay, 1990), and HEDTA for 3–10 µM (Reisert et al., 2003) free Ca^{2+}. All experiments were done at room temperature.

Circular dichroism spectroscopy

Far-UV circular dichroism (CD) spectra were recorded from 200 to 260 nm on a Chirascan-plus (Applied Photophysics) spectropolarimeter at 25°C in 1-ml quartz cuvettes (Hellma), averaging three scans with the buffer baseline and offset (recorded at 320–330 nm) subtracted (step size 1 nm, bandwidth 1 nm). CD spectra were normalized with respect to the number of amino acids, the optical path length of the cuvette, and the protein concentration as determined from the absorbance between 279 and 281 nm. Stock solutions of proteins and peptides were prepared in buffer containing 100 mM NaCl, 20 mM HEPES, and 67 µM free Ca^{2+} at pH 7.2. Ca^{2+} buffer was HEDTA. CaM wt and mutant concentrations were 29.4 µM and 29.9 µM, respectively. Peptide concentrations were 8.6 µM for ANO 1, 13.4 µM for ANO 2, and 32.3 µM for ANO ctrl. For data analysis, average spectra were calculated and normalized to the total amount of amino acids.

Bioinformatic analysis

To identify orthologous ANO genes in zebrafish, rat, mouse, and humans, we used mouse ANO sequences as queries for BLAST searches by Ensembl and NCBI. Splice site prediction was obtained from Ensembl. For sequence comparison, the RCBM and segment *c* regions from rat, mouse, human, and zebrafish were aligned using CLUSTAL. Rat sequences are depicted in Fig. 11; alignments with zebrafish are shown in Fig. S1. CaM recruitment signaling (CRS) motifs in the N terminus of ANO 1–10 were predicted using the Calmodulin Target Database (Yap et al., 2000). Bayesian phylogenetic analyses for the RCBM of rat and zebrafish orthologues were performed with MrBayes 3.0β4 (Huelsenbeck and Ronquist, 2001) with the WAG matrix (Whelan and Goldman, 2001). Metropolis-coupled Markov chain Monte Carlo sampling was performed with one cold and three heated chains that were run for 30,000 generations. Trees were sampled every 10th generation. Posterior probabilities were estimated on 2,000 trees (burnin = 1,000). The tree presented in Fig. 11 B was visualized using TreeView.

RESULTS

We used nonstationary current analysis to monitor the activation of Ca^{2+}-activated Cl^- channels and to reveal functional differences between ANO 1 and ANO 2. The channel genes from rat OE were cloned with C-terminal YFP tags. All electrophysiological recordings were obtained from HEK 293 cells transiently transfected with the respective channel DNA. Transfected cells were identified through their YFP fluorescence and selected for similar fluorescence intensity. Channel activation was triggered with 0.7–62 µM free Ca^{2+} that was included in the pipette solution of whole-cell experiments. Cl^- was the only permeant ion species present inside and outside of the cells. Currents were driven by a constant membrane voltage of −70 mV, clamped through the patch pipette. Upon opening the membrane in the pipette tip, currents of several nanoampere (nA) amplitude developed within a few seconds, reflecting the activation of Cl^- channels as a consequence of the rising intracellular Ca^{2+} concentration (Fig. 1 A). Currents were transient and

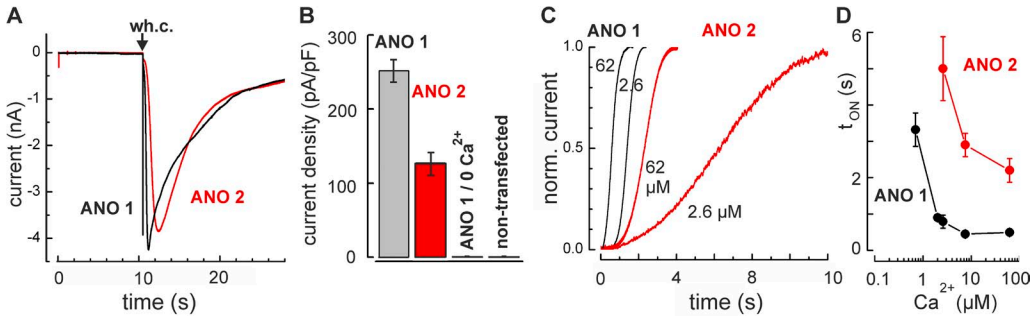

Figure 1. Nonstationary analysis of Ca^{2+}-dependent Cl^- currents. (A) Whole-cell (wh.c.) recordings at −70 mV from two HEK 293 cells expressing either ANO 1 (black) or ANO 2 (red) channels. The pipette solution contained 62 µM free Ca^{2+}. (B) Mean peak current densities from cells transfected with ANO 1 (252 ± 15.4 pA/pF; 24 cells) and ANO 2 (127 ± 14.6 pA/pF; 23 cells) channels. Control recordings without Ca^{2+} in the pipette solution or in mock-transfected cells yielded no detectable current. (C) Time course of channel activation with either 2.6 µM or 62 µM free Ca^{2+} in the pipette solution. ANO 1 channels activate faster than ANO 2 channels. (D) The activation time t_{ON}, defined as the time period from membrane disruption to 80% of the maximal current, illustrates faster Ca^{2+}-dependent activation of ANO 1. Error bars indicate mean ± SEM.

declined by ~80% within 30 s. Electrically, these currents were inward-directed (negative), but the underlying ion flux was a Cl^- efflux from the cells. Such currents did not occur in the absence of Ca^{2+} in transfected cells, nor in nontransfected cells (Fig. 1 B). At any Ca^{2+} concentration, current activation was faster in cells transfected with ANO 1 compared with ANO 2 (Fig. 1 C). A quantitative analysis of the Cl^- currents revealed that t_{ON}, the time to reach 80% of the maximal current amplitude, was Ca^{2+} dependent and displayed a shift to higher Ca^{2+} concentrations for ANO 2 with respect to ANO 1 (Fig. 1 D). Assuming that the perfusion dynamics are the same in ANO 1 cells and ANO 2 cells, the difference in t_{ON} values suggests that the transition to the open configuration occurs at lower Ca^{2+} concentrations in ANO 1 than in ANO 2. This result is consistent with the earlier finding that ANO 1 channels display higher Ca^{2+} sensitivity (Schroeder et al., 2008) than ANO 2 channels (Pifferi et al., 2009; Stephan et al., 2009).

ANO 2 channels inactivate more efficiently than ANO 1 channels

Ca^{2+}-induced currents declined within 30 s, although the Ca^{2+} concentration during whole-cell perfusion increased to a constant level. The current decline may reflect the progressive reduction of open probability, caused by a time-dependent inactivation process that may be intrinsic to channel gating. Alternatively, such a transient time course may be caused by depletion of chloride inside the cell, which would reduce Cl^- efflux. The observation that larger currents displayed a faster decline (Fig. 2, A and B) points to depletion, as larger currents caused faster reduction of the intracellular Cl^- concentration. Moreover, the Cl^- reversal voltage E_{Cl}, determined from I/V_m relations that were recorded after complete current decline, was in the range of −40 to −30 mV (Fig. 2 A, inset), which indicates an intracellular Cl^- concentration of 30–50 mM. To obtain an estimate for the dynamics of Cl^- depletion during the initial transient current, we calculated the current integral, which corresponds to the number of Cl^- ions lost through Cl^- channels during the transient current. Fig. 2 C shows the current integral obtained from a comparably small ANO 2 current with a peak amplitude near 1 nA. The current integral reaches a value of 5.96 nC after 10 s, reflecting a total efflux of 3.72×10^{10} Cl^- ions in that time period. For a spherical cell with a diameter of 10 µm (volume = 0.5 pL), this Cl^- efflux would reduce the intracellular Cl^- concentration by 120 mM. This estimate does not take into account Cl^- influx from the pipette into the cell, which we could not measure. To compensate for this Cl^- influx, we used a relatively small current for our estimate. The measured mean current amplitudes were 4.42 ± 0.25 nA (n = 24)

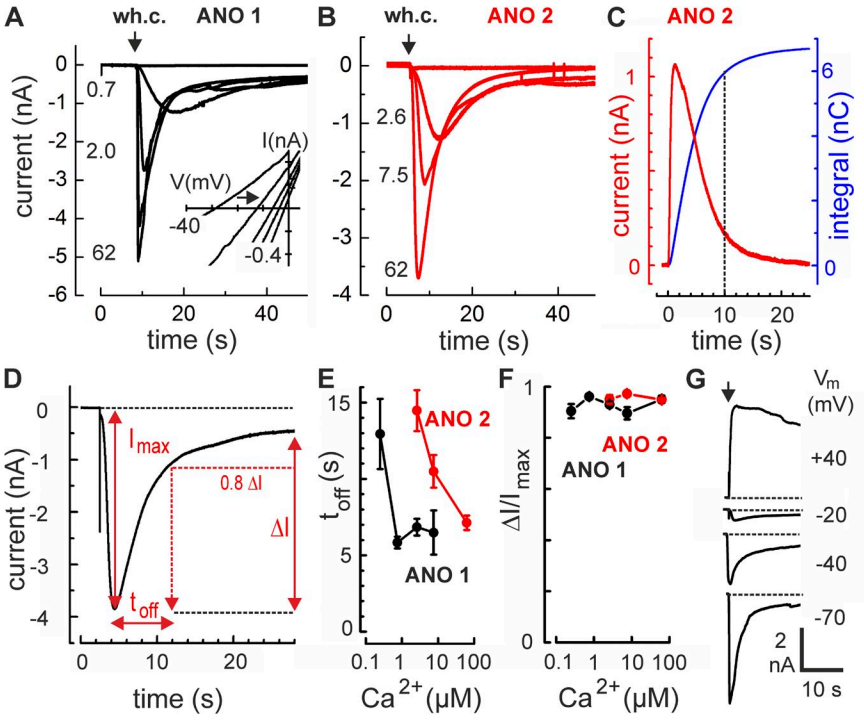

Figure 2. Cl^- depletion and the initial, rapid current decline. (A and B) Current traces at different Ca^{2+} concentrations demonstrate that larger currents cause faster current decline. Inset, current-to-voltage (I/V_m) relations obtained from −80 mV to +80 mV voltage ramps (duration, 1 s). The first ramp was applied 2 min after whole-cell (wh.c.) breakthrough. The initial currents transient lasted 28 s and reached −6.5 nA peak amplitude at −70 mV. Repeated voltage ramps at 15-s intervals caused a progressive shift of the reversal voltage from −29 mV toward 0 mV, indicating a rising intracellular Cl^- level caused by Cl^- influx during the ramp protocol. (C) The current integral (blue) calculated from the initial Cl^- current (−I(t); red), indicates the charge transfer accumulated during the rapid current transient. The current integral was used to estimate changes of intracellular Cl^- concentration, Δc, according to $\Delta c = \Delta Q/(V \times e \times L)$, where Q indicates the measured accumulated charge, V = 0.5 pL an assumed cell volume, e the elementary charge, and L the Avogadro constant. (D) Current recording depicting the parameters that characterize the current decline: maximal current, I_{max}; time for 80% of current decline, t_{off}; total extent of current decline, ΔI. (E) The speed of current decline depends on the pipette Ca^{2+} concentration and is faster in ANO 1 than in ANO 2. (F) The total extent of current decline does not depend on Ca^{2+} concentration. Error bars indicate mean ± SEM. (G) Whole-cell recordings from four different cells that express ANO 1 illustrate that the rapid decline of the initial current is observed at negative voltages, but not at +40 mV. The arrow indicate whole cell breakthrough.

for ANO 1 and 2.14 ± 0.18 nA ($n = 23$) for ANO 2, which suggests a two- to fourfold higher rate of Cl^- efflux than used for our estimate. Thus, the large Ca^{2+}-dependent Cl^- currents may cause a pronounced decrease of the intracellular Cl^- concentration, an effect that explains the decline of Cl^- currents after a few seconds. The time course of current decline depended on the Ca^{2+} concentration (Fig. 2, D and E), whereas the total extent of current decline did not (Fig. 2 F). These observations suggest that a final level of Cl^- depletion is reached earlier upon rapid channel activation at high Ca^{2+}. No rapid current decline was seen at positive voltages when the current was carried by Cl^- ions entering the cell from the bath (Fig. 2 G). The bulk Cl^- concentration in the bath is not strongly affected by the Cl^- currents. Consequently, Cl^- depletion cannot occur outside of the cell. Collectively, these data are consistent with the view that the initial, rapid current decline in our experiments was caused by intracellular Cl^- depletion.

To record Cl^- currents without producing Cl^- depletion, we applied a series of 1-s voltage ramps from −70 to +70 mV, 4 s apart, using Ca^{2+} concentrations that fully activated ANO channels within ∼1 s. In this protocol, the durations of Cl^- influx and Cl^- efflux are virtually equal, and, in the absence of pronounced current rectification (Fig. 3 A), any net change of intracellular Cl^- concentration remains small. ANO 1 currents declined only slowly, showing a decrease at +70 mV of 23 ± 7% ($n = 5$) over 80 s (Fig. 3 D). In contrast, ANO 2 currents decayed almost completely (86 ± 8.2%; $n = 7$) over the same time period (Fig. 3, B and E). Currents at negative voltages decreased faster than at positive voltages, giving rise to a progressive rectification of the I/V_m relation. The rectification ratio ($I_{+70\ mV}/I_{-70\ mV}$) strongly increased in ANO 2, but not in ANO 1 (Fig. 3 C).

The time course of current decline in ANO 2 could be fitted with a single-exponential function and displayed pronounced voltage dependence, with fastest decline at negative membrane voltages (Fig. 3 F). These results demonstrate that, in both ANO 1 and ANO 2 channels, there is a delayed loss of Cl^- channel activity that is not caused by Cl^- depletion. This process is considerably faster and more pronounced in ANO 2 compared with ANO 1.

To further characterize this process, we examined whether it depends on current flow through the channel or if it also occurs in the absence of Cl^- flux. We preloaded the cells for 60–90 s with 7.5 μM Ca^{2+} at a holding voltage of 0 mV. In the absence of an electrical driving force, only small, transient outward currents, driven by the initial Cl^- concentration difference between cytosol (estimate from E_{Cl}: 80–100 mM Cl^-), bath, and pipette (150 mM), were detected (Fig. 4 A, left traces). At the end of the preloading phase, equilibration between cytosol, pipette, and bath medium was reached, and we turned the Cl^- current on by switching the membrane voltage to −70 mV. Channels in ANO 1–expressing cells displayed large, transient currents (Fig. 4 A, black trace, 9 cells), whereas no current was observed in ANO 2–expressing cells (Fig. 4 A, red trace, 12 cells). Thus, after preloading, ANO 1 channels were active, whereas ANO 2 channels were completely inactive. In particular, inactivation of ANO 2 was Ca^{2+}-dependent and did not depend on ion flow through the channel pore. Our protocol did not allow us to systematically examine the question of whether this ANO 2 inactivation was a reversible process, because we could not remove Ca^{2+} from the cells. However, on a few occasions, we observed resealing of the plasma membrane, indicated by an increase of access resistance and a drop

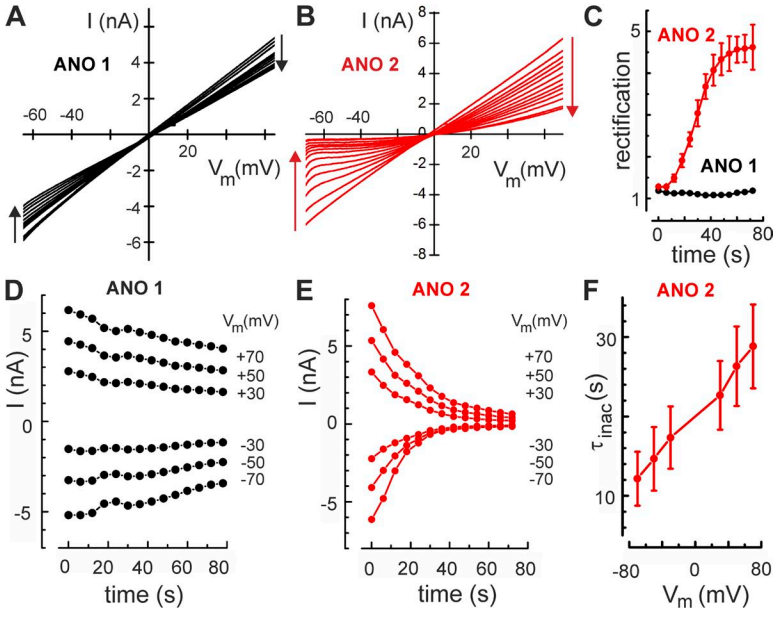

Figure 3. Inactivation of ANO 2 currents. (A) Current-to-voltage (I/V_m) relations, obtained from 14 consecutive 1-s voltage ramps recorded at 5-s intervals from an ANO 1–expressing cell show a slow decline of whole-cell current in the absence of Cl^- depletion. (B) The same experimental protocol reveals a faster current decline in a cell expressing ANO 2 channels. (C) Over the 80-s duration of the experiment, the current rectification ratio ($I_{+70\ mV}/I_{-70\ mV}$) steadily increased in ANO 2, but remained near unity (no rectification) in ANO 1. (D) The time course of current decline at the indicated voltages reveals a slow inactivation process in ANO 1, with ∼10% loss over 80 s. (E) In an ANO 2–expressing cell, the time course of current decline illustrates almost complete inactivation within 60 s. (F) The time constant of the single-exponential decay of ANO-2 currents was voltage dependent (means of five cells). Error bars indicate mean ± SEM.

of membrane capacitance, after current recording. In these cases, a second current transient was monitored after 2–3 min upon a second whole-cell breakthrough. This observation indicates that ANO 2 inactivation is indeed a reversible process.

Inactivation, here defined as a loss of channel activity in the continuous presence of Ca^{2+}, should be accompanied by a change of gating activity, as the channels reduce their open probability. This can be monitored by the current variance during nonstationary current analysis. ANO 2 current recordings displayed two distinct phases of increased current noise: one during the rise of the current and one during its decline (Fig. 4 B, sections in red boxes). The two phases marked, respectively, the increase and the decrease of open probability. It is instructive to inspect the precise temporal relation of current and variance in these recordings. In the activation phase (Fig. 4 C, phase A), the current variance σ^2 peaked when the current amplitude reached its half-maximal level. The peak variance signifies the passage of the open probability P_o through 0.5, the level of maximal gating activity, as P_o rises from zero toward unity (Sigworth, 1980). During the ensuing rapid current decline, which is caused by Cl^- depletion (Fig. 4 C, phase D), the variance stays near zero, indicating that P_o remains high. The second noisy phase occurs during the elongated tail of the current transient (Fig. 4 C, phase inactivation). The variance peaks again as P_o returns from unity to zero. This latter process is termed inactivation. According to this concept, the changes of current variance over time are determined solely by changes in P_o. A fit of the equation $\sigma^2(t) = NP_o(t) \times [1 - P_o(t)]\, i^2$ confirms this notion (Fig. 4 C, blue line). N represents a constant number of channels and i the constant single-channel current at $V_m = -70$ mV (see legend to Fig. 4 C). With P_o as the only time-dependent variable, the time course of the current variance is well approximated. Thus variance analysis supports the view that the first, rapid decline of ANO 2 currents was caused by intracellular Cl^- depletion, followed by channel inactivation within 30 s after activation.

Activation of ANO 1 and ANO 2 involves an N-terminal domain

It is not yet understood through which mechanism Ca^{2+} opens ANO 1 and ANO 2 channels and how ANO 2 is inactivated, although several regions in the ANO proteins clearly contribute to setting the channel's Ca^{2+} sensitivity (see Discussion). It is unlikely that Ca^{2+}-dependent kinases trigger activation, because channels open instantaneously in inside-out patches when Ca^{2+} is added rapidly in the absence of ATP (Reisert et al., 2003; Pifferi et al., 2009; Stephan et al., 2009; Xiao et al., 2011; Yu et al., 2012). Moreover, we have performed a series of nonstationary current recordings in the presence of the membrane-permeable protein kinase inhibi-

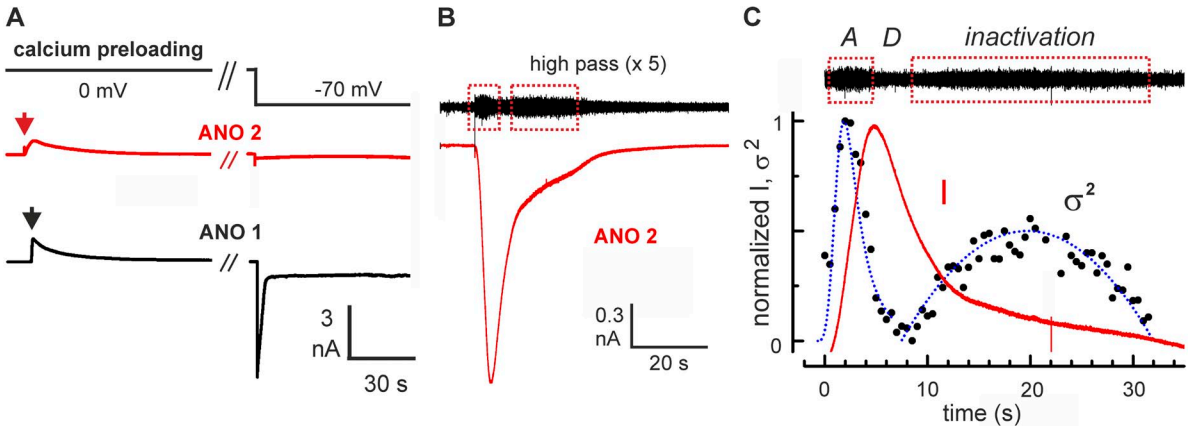

Figure 4. The Ca^{2+}-dependent inactivation of ANO 2 affects gating. (A) Ca^{2+}-preloading experiments with ANO 1 and ANO 2 channels. During preloading with 7.5 µM free Ca^{2+} at 0 mV, channels were activated and conducted small, transient outward currents during equilibration of cytosol, pipette, and bath solution (left traces). Subsequent application of −70 mV induced current in ANO 1–expressing cells. In contrast ANO 2–expressing cells showed no Cl^- current as a consequence of complete ANO 2 inactivation during preloading (right traces). Arrows indicate whole cell breakthrough. (B) Nonstationary current recording at −70 mV from a cell expressing ANO 2 channels. After high-pass filtering of the data, two episodes of increased current noise are discernible (black trace; boxes). (C) Gating activity during the current transient. The peak of current variance (dots) during cell perfusion with 7.5 µM Ca^{2+} preceded the peak current amplitude (normalized current; red line). The maximal variance coincided with the half-maximal current in the activation phase (depicted as "*A*"). During the ensuing phase of Cl^- depletion (depicted as "*D*"), the variance remained unchanged at a very low value, reflecting the persistent low level of gating activity in the fully activated channels. About 10 s after the start of cell perfusion, the current variance increased again and reached a second peak within ∼8 s (inactivation). This second peak reflects channel inactivation, as the open probability returned from near unity at t = 8 s to near 0 at t = 32 s. The blue line results from a fit of the equation $\sigma^2(t) = NP_o(t) \times [1 - P_o(t)] \times i^2$ to the normalized variance data, with $\sigma^2(t)$ for the normalized variance. $n = 100$, the number of channels; $P_o(t)$, the open probability; i = 0.14 pA, the single-channel current. The fit demonstrates that the time course of the current variance can be described with P_o as the only variable, a characteristic feature of gating effects.

tor staurosporine (0.2–2 µM, 5–50 min, applied to the bath solution) and did not detect any effect on channel activation or inactivation (6 cells expressing ANO 1, 18 cells expressing ANO 2; unpublished data). In an earlier study, we obtained evidence for CaM effects on the Ca^{2+} sensitivity of Ca^{2+}-activated Cl^- channels expressed in a cell line from OE (Kaneko et al., 2006). Moreover, a study of ANO 1–expressing HEK 293 cells provided evidence for a direct interaction of CaM with ANO 1 and for a pivotal role of CaM in channel activation (Tian et al., 2011). Finally, a recent study revealed that binding of Ca^{2+}/CaM affects the ion selectivity of ANO 1 (Jung et al., 2013).

To find out whether CaM is involved in channel activation, we first examined the effects of two membrane-permeant CaM inhibitors. We reduced the availability of CaM for regulatory processes by applying trifluoperazine (TFP) or J-8, which bind CaM (Craven et al., 1996; Feldkamp et al., 2010). Neither of the two compounds was effective in blocking the activation of ANO 1 or ANO 2 channels. Bath application of 20 µM TFP or 50 µM J-8 for 10–70 min did not significantly reduce the current densities from the control values observed in the nonstationary current experiments (ANO 1, 252 ± 15.4 pA/pF; ANO 2, 127 ± 14.6 pA/pF). Mean current densities for TFP were 277 ± 52 pA/pF (6 cells) with ANO 1 and 166 ± 24 pA/pF (6 cells) with ANO 2. With J-8, we measured 271 ± 56 pA/pF (3 cells) with ANO 1 and 156 ± 52 pA/pF (11 cells) with ANO 2 channels. This resistance against CaM antagonists points to two alternatives: Either CaM is not involved in channel activation, or CaM is stably associated with the channel protein and not accessible for the inhibitors.

In the case of stable association, the interaction between CaM and the channels may either be independent of Ca^{2+} (binding of apo-CaM), or may require low concentrations of Ca^{2+} for binding. To test for these possibilities, we overexpressed CaM mutants that compete with endogenous CaM for binding to the channels. These mutants have been instrumental in revealing CaM regulation in various ion channels (Xia et al., 1998; Lee et al., 1999; Peterson et al., 1999; Zühlke et al., 1999; DeMaria et al., 2001; Erickson et al., 2001; Pitt et al., 2001; Erickson et al., 2003; Mori et al., 2004; Kasri et al., 2006; Shen et al., 2006; Yang et al., 2006; Dick et al., 2008; Stroffekova, 2008). We used CaM mutants with all four Ca^{2+} sites disabled (CaM1234), as well as mutants with disabled binding sites in the N-terminal (CaM12) or C-terminal lobe (CaM34). The results of these experiments are shown in Fig. 5 A. As a control experiment, wt CaM was transfected together with ANO 1. This reduced the mean ANO 1 current only slightly, possibly through the increased Ca^{2+} buffer capacity at elevated cytosolic CaM concentrations. Overexpression of Ca^{2+}-free CaM1234 had no significant effect on current densities, which indicates that no Ca^{2+}-independent, apo-CaM–mediated process contributes to channel regulation. In contrast, the mutants CaM12 and CaM34, containing single intact lobes, caused a decrease of ANO 1 currents by 50% (Fig. 5 A). Thus, in the presence of Ca^{2+}, CaM indeed affects channel activity. CaM12 and CaM34 may compete with endogenous CaM for Ca^{2+}-dependent regulation. Thus, our results indicate that CaM is involved in channel regulation, and that it is associated with the channels in a Ca^{2+}-dependent manner.

The overexpression of CaM mutants is an indirect assay for CaM-mediated regulation, but provides no direct proof for CaM binding. To test for in vivo interaction of ANO channels with CaM, we precipitated both proteins from lysates of stably transfected HEK 293 cells using an antiserum directed against the C-terminal YFP tag of both channels (see Materials and methods). CaM coprecipitated with ANO 1 and ANO 2 (Fig. 5 B), as was shown for ANO 1 previously (Tian et al., 2011; Jung et al., 2013). CaM was confirmed by mass spectrometry of the respective bands (five unique peptides identified). This result confirms that the channels bind CaM. It does not, however, provide any indications as to the site and to the affinity of this interaction. To locate a possible association site, we searched for putative CaM-binding domains in those sequences of ANO 1 and ANO 2 that may be involved in channel gating. A previously identified N-terminal CaM-binding domain CAMBD2/CBM1 was found to be dispensable for channel activation (Tian et al., 2011; Jung et al., 2013). We also confirmed that a second N-terminal candidate motif (CaM-binding domain 1 [CAMBD1]; Tian et al., 2011) could be deleted without loss of channel function. This site is encoded by a separate exon of ANO 1 (segment *b*; Ferrera et al., 2009). The ANO 1 splice variant that misses CAMBD1 displays a particularly high Ca^{2+} sensitivity (Ferrera et al., 2009). In our hands, ANO 1 channels without CAMBD1 could be activated with Ca^{2+} concentrations between 0.7 µM to 62 µM (unpublished data). CAMBD1 is not present in ANO 2. We identified a different CRS motif in the N terminus, predicted by the Calmodulin Target Database. The prediction is based on positioning and content of hydrophobic residues, hydropathy, residue weight and charge, propensity to form α-helices, and occurrence of characteristic residues (Yap et al., 2000). The CRS motif is located in the N terminus and is highly conserved between ANO 1 and ANO 2 channels (alignments for fish and mammals are shown in Fig. S1). We refer to the CRS motif as "regulatory CaM-binding motif" (RCBM), denoting its putative role in channel regulation (Fig. 5 C). The deletion of the RCBM sequence from ANO 1 or ANO 2 produced nonfunctional proteins (unpublished data). In comparison to canonical CaM-binding domains, the RCBM shows an unusual feature: two helical regions (predicted by the Jpred3 secondary structure prediction server), interrupted by a single proline, and flanked by two identical

basic motifs. This arrangement is reminiscent of the CaM target motif in the skeletal muscle myosin light-chain kinase (Peersen et al., 1997). To find out whether the RCBM binds CaM in vitro, we synthesized peptides corresponding to the RCBM sequence of ANO 1 and ANO 2. A mutant control peptide (ANO ctrl) was designed that lacked any amphipathic structure to disable CaM binding.

We monitored changes in secondary structure using CD spectroscopy to characterize the binding of CaM to the test peptides. We recorded far-UV spectra in the presence of Ca^{2+} (67 µM free Ca^{2+}) for each peptide in the presence and absence of CaM (Fig. 5 D). The recorded CD spectra were compared with hypothetical spectra that were calculated for a noninteracting peptide/CaM mixture. Any difference between these two spectra indicates conformational changes associated with binding. We observed such a difference for both ANO 1 and ANO 2 peptides (Fig. 5 D, asterisks), but not with the control peptide. For both peptides mixed with the Ca^{2+}-insensitive CaM mutant CaM1234 at 67 µM Ca^{2+}, recorded and calculated spectra matched perfectly, indicating the absence of an interaction with CaM1234 (Fig. 5 E). These data provide a qualitative evidence for the interaction between the RCBM peptides of ANO 1 and ANO 2 with CaM in the presence of Ca^{2+}.

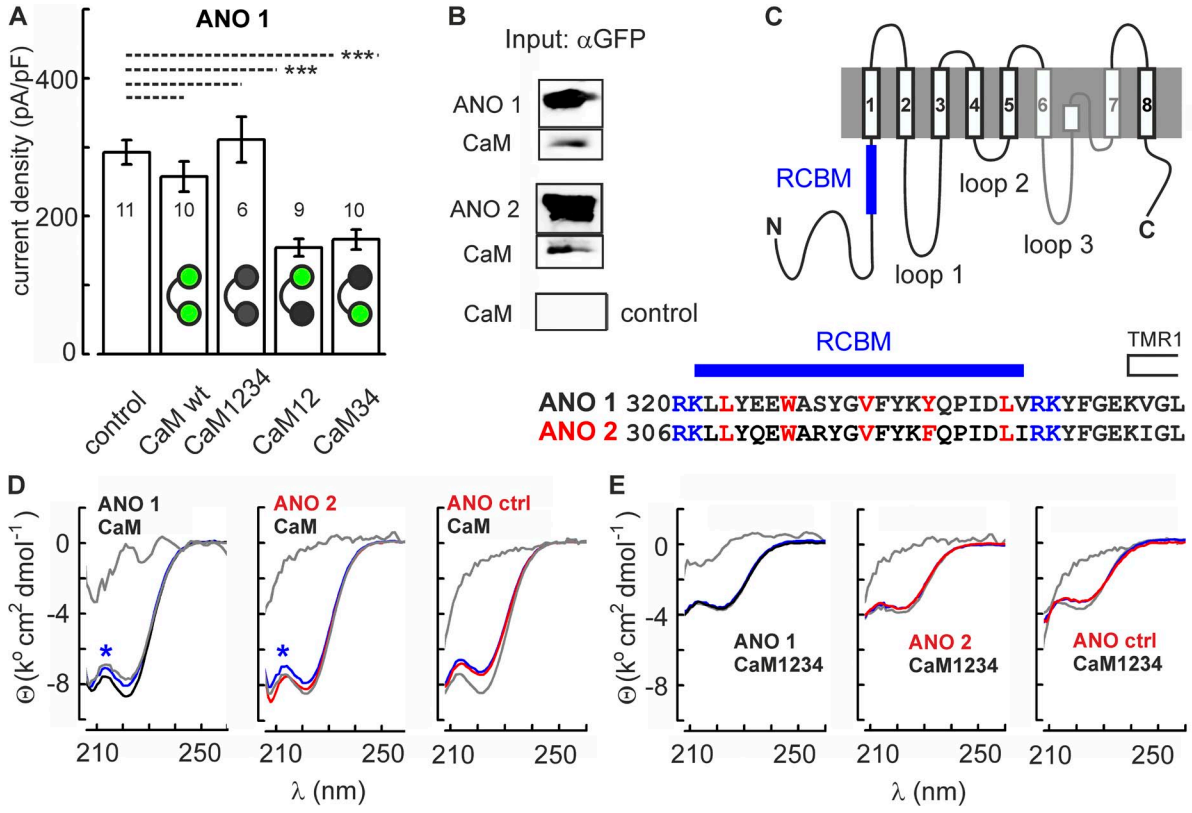

Figure 5. CaM is involved in channel activation. (A) Overexpression of CaM mutants in HEK 293 cells transfected with ANO 1 channels. Wt CaM or CaM with all four Ca^{2+}-binding sites disabled (CaM1234) had no significant effect on the Ca^{2+} dependent Cl^- current. CaM mutants with either the N-terminal (CaM12) or C-terminal (CaM34) Ca^{2+}-binding sites disabled reduced the ANO 1 current by 54%. Dumbbell symbols depict the two Ca^{2+}-binding lobes of the CaM molecule (green, intact; gray, disabled). ***, $P < 0.001$, unpaired *t* test. Numbers on bars indicate the numbers of experiments. Error bars indicate mean ± SEM. (B) Coprecipitation of CaM with ANO 1 and ANO 2, precipitated with an anti-GFP antiserum. YFP was fused to the ANO channels as a tag. In HEK 293 cells transfected with YFP alone, no CaM coprecipitated with YFP (control). (C) Current topology model for ANO Ca^{2+}-activated Cl^- channels according to Yu et al. (2012). The channel protein probably has eight TMRs with cytosolic N and C termini. The structure of the pore region that includes TMRs 6 and 7 as well as a reentrant loop has not yet been definitively clarified. The N-terminal region contains a CRS motif, here referred to as regulatory CaM-binding motif (RCBM), which is encoded by exon 9 in human ANO 1 (Ferrera et al., 2009). The sequence alignment demonstrates a high degree of similarity between ANO 1 and ANO 2 in this motif. Red letters indicate residues predicted to form the hydrophobic side of the amphipathic helix. The flanking basic motifs are shown in blue. TMR1, transmembrane region 1. (D) Averaged ($n = 3$) and normalized CD spectra in the presence of 67 µM Ca^{2+} are shown for mixtures of CaM and the test peptides (black lines for ANO 1 and red lines for ANO 2 and ANO control [ANO ctrl]) and for their weighted averages (blue lines). Spectra for the binding partners alone (with 67 µM Ca^{2+}) are shown in gray (top trace, test peptide; bottom trace, CaM). The control peptide ANO ctrl contained glutamate in positions 2, 6, 15, and 20 of the RCBM sequence. Blue asterisks denote a significant deviation of the calculated spectrum from the measured spectrum of the mixture, which is indicative of an interaction between the test peptides and CaM. (E) Control CD spectra show that neither test nor control peptides bound to Ca^{2+}-insensitive CaM mutant CaM1234 in the presence of Ca^{2+}.

To further quantify this interaction, we tagged the peptides C-terminally with Badan, a conformation-sensitive fluorescent probe (Gangopadhyay et al., 2004; Ungerer et al., 2011). Fluorescence emission spectra of tagged RCBM peptides were recorded at increasing Ca^{2+} concentrations in the presence or absence of CaM (Fig. 6). In the absence of CaM, no Ca^{2+}-dependent changes were observed with the control peptide (Fig. 6 A), or with the two RCBM peptides (Fig. 6, B and C, left). Thus, peptide conformation is not directly affected by Ca^{2+}. However, in the presence of CaM and upon Ca^{2+} addition, the fluorescence maxima shifted to blue and the fluorescence intensities increased for both RCBM peptides. This indicates CaM binding (Fig. 6, B and C, center). Hill-fits to the blue-shift data revealed a high Ca^{2+} sensitivity and a pronounced difference between the two peptides (Fig. 6, B and C, right). With the ANO 1 peptide, the concentration for half-maximal shift, EC_{50}, was 0.09 ± 0.01 µM Ca^{2+} (n = 3), with a Hill coefficient of 3.2 ± 0.6. The ANO 2 peptide yielded an EC_{50} of 0.23 ± 0.01 µM Ca^{2+} (n = 3) and a Hill coefficient of 2.8 ± 0.2. Thus, the association of CaM with the RCBM peptides is Ca^{2+}-dependent, cooperative, and occurs at submicromolar Ca^{2+} concentrations. Furthermore, despite the similarity of amino-acid sequences, the ANO 2 peptide responds with a more vigorous conformational change compared with ANO 1. These results suggest that CaM is associated with the RCBM sequences at low

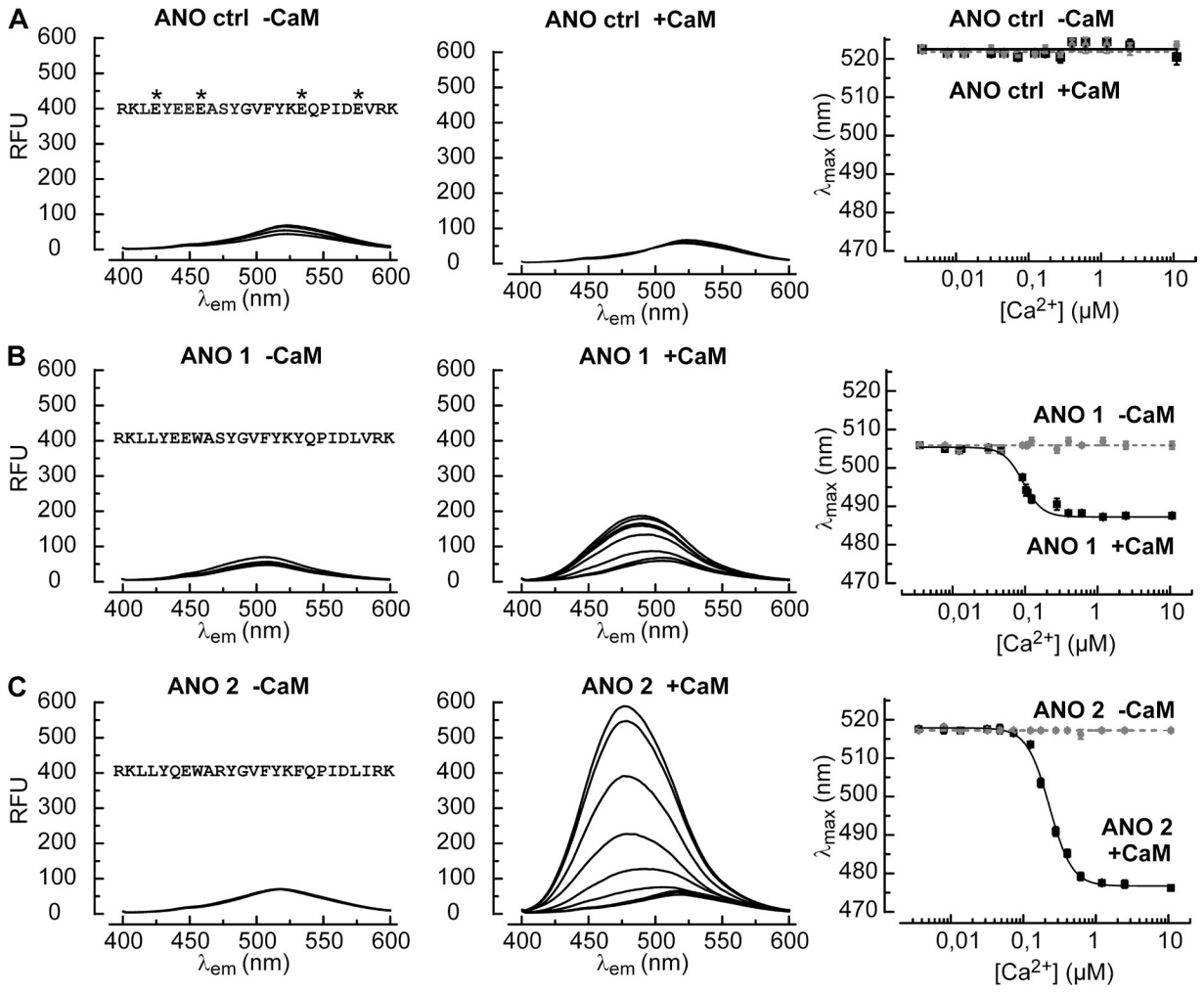

Figure 6. CaM binds to RCBM peptides at low Ca^{2+} concentrations. (A) Fluorescence emission spectra of the Badan-labeled control peptide (3 µM) without CaM (−CaM, left) and in the presence of 1.5 µM CaM (+CaM, middle). The free Ca^{2+} concentrations ranged from 0.007 to 10 µM. Spectra did not change with the Ca^{2+} level. Asterisks indicate the four point mutations used to perturb CaM binding. The diagram on the right displays the dependence of the wavelength for maximal emission (λ_{max}) on the Ca^{2+} concentration with (solid line) and without (broken line) CaM. Error bars indicate mean ± SEM. (B) The Badan-labeled RCBM peptide corresponding to ANO 1 responds to increasing Ca^{2+} in the presence of CaM with a blueshift of the fluorescence emission spectrum and an increase in fluorescence intensity (middle). The dependence of λ_{max} on the Ca^{2+} concentration (right) is described by a Hill function (solid line) with an EC_{50} of 0.09 ± 0.01 µM Ca^{2+} (n = 3) and a Hill coefficient of 3.2 ± 0.6. (C) The ANO 2 peptide displays a stronger response to Ca^{2+} in the presence of CaM than the ANO 1 peptide, both with respect to the blue-shift of λ_{max} and to the fluorescence intensity. A fit of the Hill function yielded an EC_{50} of 0.23 ± 0.01 µM Ca^{2+} (n = 3) and a Hill coefficient of 2.8 ± 0.2 (right).

Ca^{2+} levels, and only dissociates when Ca^{2+} concentrations drop below 0.1–0.2 µM.

The RCBM sequence contains five hydrophobic residues (Fig. 5 C), which together constitute the hydrophobic face of the amphipathic motif. Replacing the first two and the last two residues with glutamate completely abolished CaM binding (ANO ctrl: m2,6,15,20; Fig. 6 A). However, CaM binding persisted when only two residues were replaced (m2,6 or m15,20). The ANO 1 peptide responded similarly to the m2,6 mutation and the m15,20 mutation (Fig. 7 A). The EC_{50} for CaM binding shifted 100-fold to 12 ± 1.4 µM (n = 3) with a Hill coefficient of 1.8 ± 0.4 in the m2,6 mutant, and to 15.2 ± 2.1 µM (n = 3) with a Hill coefficient of 2.2 ± 0.3 in the m15,20 mutant. In contrast, the ANO 2 peptide responded differently to the two mutations (Fig. 7 B). Although the m2,6 mutant displayed a 30-fold shift to an EC_{50} of 6.0 ± 0.8 µM (n = 3) with a Hill coefficient of 2.5 ± 0.5, the m15,20 mutant was shifted only to 0.6 ± 0.11 µM (3) with a Hill coefficient of 2.2 ± 0.7. These results demonstrate that, in both RCBM peptides, the intact amphipathic structure supports cooperative, high-affinity binding of Ca^{2+}/CaM. However, although ANO 1 requires the integrity of the entire sequence, ANO 2 requires only the proximal section of the segment for high-affinity binding. These results may indicate that the RCBM sequence of ANO 2 is a bipartite structure with two distinct sites of interaction for Ca^{2+}/CaM. However, the question of RCBM/CaM stoichiometry has to be solved in the future through NMR, calorimetric studies, or sedimentation analyses.

To examine the interaction of the CaM mutants with the RCBM peptides, we recombinantly produced and purified CaM12, CaM34, and CaM1234 (Ungerer et al., 2011). Both CaM12 and CaM34 bound to the RCBM peptides with a similar affinity as the wt protein (EC_{50} values increased only two to fourfold; Fig. 7, C and D). In accordance with CD data, the Ca^{2+}-insensitive mutant CaM1234 did not bind over a broad range of Ca^{2+} concentrations. Thus, high-affinity binding of Ca^{2+}/CaM to the RCBM peptides is mediated by either of the two lobes of the CaM molecule.

To find out whether the integrity of the RCBM domain is also necessary for channel gating in vivo, we introduced point mutations into the RCBM sequence of ANO 1 and ANO 2 channels. Fig. 8 A shows the respective mutations, and Fig. 8 B illustrates the expression patterns of wt and mutated channels in HEK 293 cells. ANO 1 wt channels displayed a highly polarized expression that appeared to be confined to the plasma membrane. All RCBM mutations tested in ANO 1 perturbed this targeting process to some extent, so that much of the mutant ANO 1 protein was located in intracellular structures (Fig. 8 B). In ANO 2 channels,

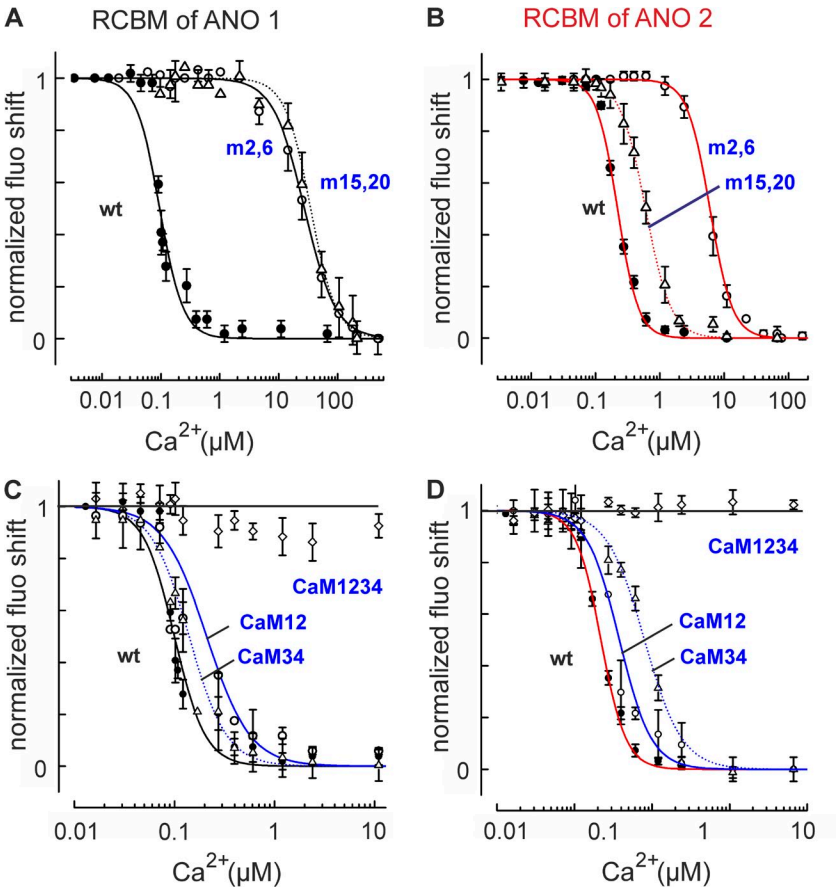

Figure 7. RCBM peptides support both high-affinity and low-affinity binding of Ca^{2+}/CaM. (A) Dose–response relations for the binding of Ca^{2+}/CaM to Badan-labeled ANO 1 RCBM peptide. Replacing nonpolar residues in the proximal (m2,6) or distal (m15,20) sections of the RCBM sequence induces a shift of the dose response relation to 100-fold higher Ca^{2+} concentrations. (B) In the ANO 2 peptide, mutation of the proximal section caused a 30-fold right-shift of the dose–response relation, whereas the distal mutations caused only a small shift into the same direction. (C) Ca^{2+} dependence of the association of CaM mutants with the ANO 1 peptide. Both the N-terminal lobe of CaM (intact in CaM34) and the C-terminal lobe (intact in CaM12) are able to support high-affinity binding to the RCBM peptide. The Ca^{2+}-free CaM mutant CaM1234 does not bind. (D) The single-lobe CaM mutants also bind with high affinity to the RCBM peptide of ANO 2. Error bars indicate mean ± SEM.

even the wt protein produced a mixed plasma membrane/intracellular signal, and this was not changed by the RCBM mutations. The mutant effects on ANO 1 expression may suggest that the RCBM sequence in ANO 1 plays a role in membrane targeting. To find out whether mutant ANO 1 channels reach the plasma membrane at all, we recorded Ca^{2+}-induced currents from cells expressing the mutants. Ca^{2+}-dependent currents were seen in the m11,15 mutant, but not in the m2 and m6 mutants (Fig. 8 C). Thus, despite its effect on membrane targeting of ANO 1, the m11,15 mutant did not prevent functional channels from inserting into the plasma membrane. This raises the question of whether the m2 and m6 mutants, which produced no current in ANO 1 and ANO 2 (Fig. 8 D), are also present in the plasma membrane, but cannot be activated by Ca^{2+}. To address this question, we used the recent finding that ANO 1 channels can be opened by strong positive voltages, even in the absence of Ca^{2+} (Xiao et al., 2011). Applying +200 mV membrane voltage to cells kept in Ca^{2+}-free solution, we recorded a net current density of 69.6 ± 5.2 pA/pF (11 cells) from cells expressing ANO 1 wt (Fig. 8 E). In cells expressing the RCBM mutations, net current densities were reduced to 6.2 ± 2.2 pA/pF (9 cells) with m2, to 15.7 ± 4.2 pA/pF (10 cells) with m6, and to 9.0 ± 2.7 pA/pF (12 cells) with m11,15. Thus, voltage-induced, Ca^{2+}-independent current densities in the RCBM mutants were much smaller compared with ANO 1 wt, presumably because fewer mutant channels reached the plasma membrane. However, current densities of the mutants differed significantly from the mock-transfected cells (Fig. 8 F), proving that some mutated ANO 1 channels were indeed present in the plasma membrane. These channels

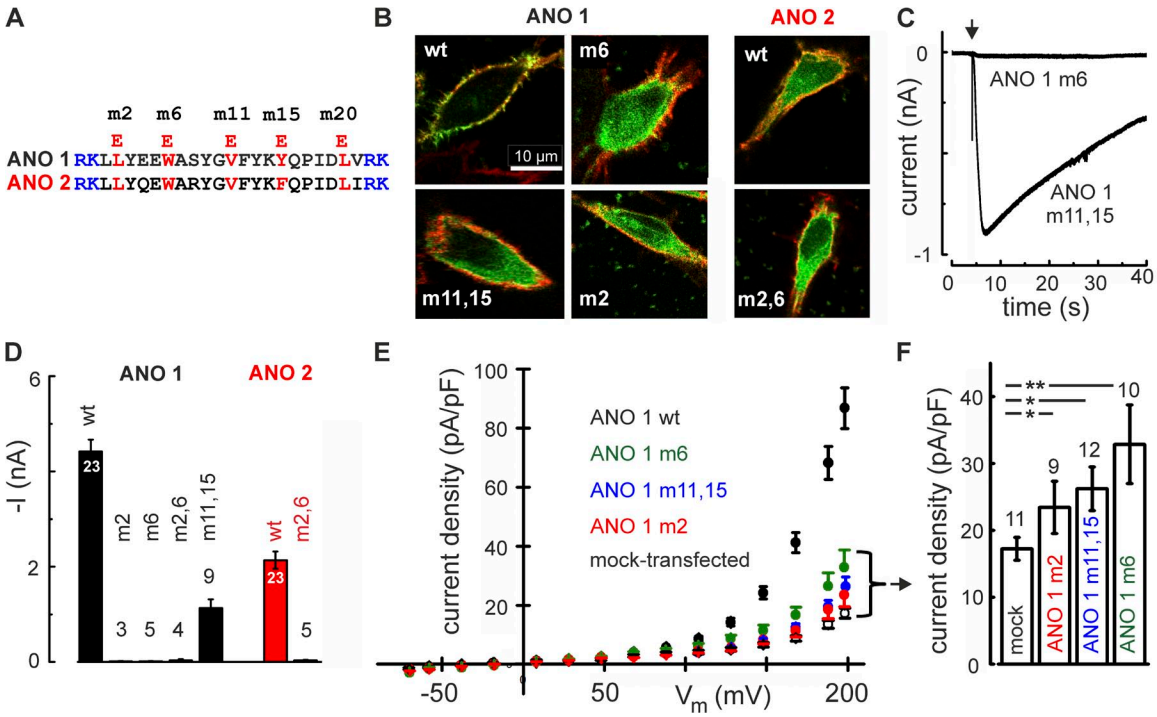

Figure 8. Functional consequences of RCBM mutations in the channel proteins. (A) RCBM sequences of ANO 1 and ANO 2 with the positions of four point mutations used to perturb CaM binding. In each mutant, a hydrophobic residue was replaced by a charged glutamate. The two flanked basic motifs of the RCBM sequence are highlighted in blue. (B) Point mutations in the RCBM sequence of ANO 1 interfere with membrane targeting. Cell surfaces are labeled with tetramethyl rhodamine–conjugated wheat germ agglutinin (red) and ANO-1 proteins with YFP (green). Although ANO 1 wt displays an almost exclusive plasma membrane signal, the immunosignals from ANO 1 mutants and from ANO 2 wt are also strong inside the cell. The ANO 2 expression pattern appears unaffected by the point mutations m2,6. (C) Mutations in the distal section of the RCBM sequence of ANO 1 (m11,15) leave the channel functional, although membrane targeting is compromised. The more proximal mutation m6 renders the channel unresponsive to 67 µM Ca^{2+}. (D) Ca^{2+}-dependent activation is blocked by mutations m2 and m6. Mean current amplitudes at 7.5 µM Ca^{2+} are shown for point mutations introduced to the proximal section of the RCBM sequence in ANO 1 and ANO 2 (m2, m6). Distal mutations (m11,15) leave the channels responsive to Ca^{2+}. The reduced current amplitude is consistent with the impaired plasma-membrane targeting shown in B. Numbers on the bars indicate numbers of experiments. (E) Ca^{2+}-independent channel activation of ANO 1 in Ca^{2+}-free solution is detected at strong positive voltages in ANO 1 wt channels. Mutant channels show reduced current density, but currents are detectable. (F) Statistical analysis of voltage-activated currents in Ca^{2+}-free solution. For all RCBM mutants tested, the current densities at +200 mV were significantly larger than in mock-transfected control cells (**, $P < 0.01$; and *, $P < 0.05$; unpaired *t* test), indicating that all mutants are expressed in the plasma membrane. Mean current densities are reduced by ~70% with respect to the ANO 1 wt (black symbols in E), probably reflecting the impaired plasma-membrane targeting. Error bars indicate mean ± SEM.

had retained the ability to open at positive voltages, but the m2 and m6 mutants could no longer be activated by Ca^{2+}. Collectively, the consistent effects of m2,6 mutations on peptide binding and channel function suggest that Ca^{2+}/CaM-binding to the proximal section of the RCBM sequence is a necessary step in channel activation. A proof of in vivo CaM–RCBM interaction has yet to be obtained from future biochemical studies.

Inactivation of ANO 2 channels is mediated by CaM

If the proximal section of the RCBM sequence is involved in channel activation, what is the role of the distal part in ANO 2? And why is the integrity of the distal part apparently not necessary for high-affinity binding to the RCBM peptide of ANO 2 (Fig. 7 B)? The extended sequence of the RCBM may indicate that a bipartite domain for CaM binding may serve two distinct functions in channel regulation. We tested whether the inactivation behavior observed only in ANO 2 may be linked to the distal section of the RCBM. The m15,20 mutant channels of ANO 2 were activated by Ca^{2+}, produced smaller whole-cell currents, and displayed impaired inactivation (Fig. 9 A). Unlike in wt ANO 2, the kinetics of current decline varied strongly between individual cells (Fig. 9 B). We did not measure inactivation with the characteristic time constant of wt ANO 2 channels (12.2 ± 3.4 s at −70 mV) in any of the cells expressing these mutants. Inactivation was slowed down and no longer followed a single-exponential time course. Inactivation was also incomplete: the current ratio I_e/I_s (with I_e representing the current amplitude at −70 mV at the end of the inactivation phase, and I_s at its start) was strongly increased in cells expressing m15,20 (Fig. 9 C). This impaired inactivation may be indicative of a role of CaM in inactivation, as it is induced by a defect in the RCBM sequence. This idea is supported by the finding that CaM inhibitors were effective in our inactivation assays. Inactivation of ANO 2 currents was completely suppressed by 20 µM TFP (4 cells) and by 50 µM J-8 (9 cells). In the presence of either compound, no channel inactivation was observed in nonstationary current recordings (Fig. 9 D).

Our results suggest that ANO 2 inactivation is mediated by CaM. As the inactivating CaM is accessible to the inhibitors, it does not appear to be stably associated with the channels, but rather to bind to ANO 2 at elevated Ca^{2+} concentrations. Because the RCBM sequence of the noninactivating ANO 1 channel has a slightly

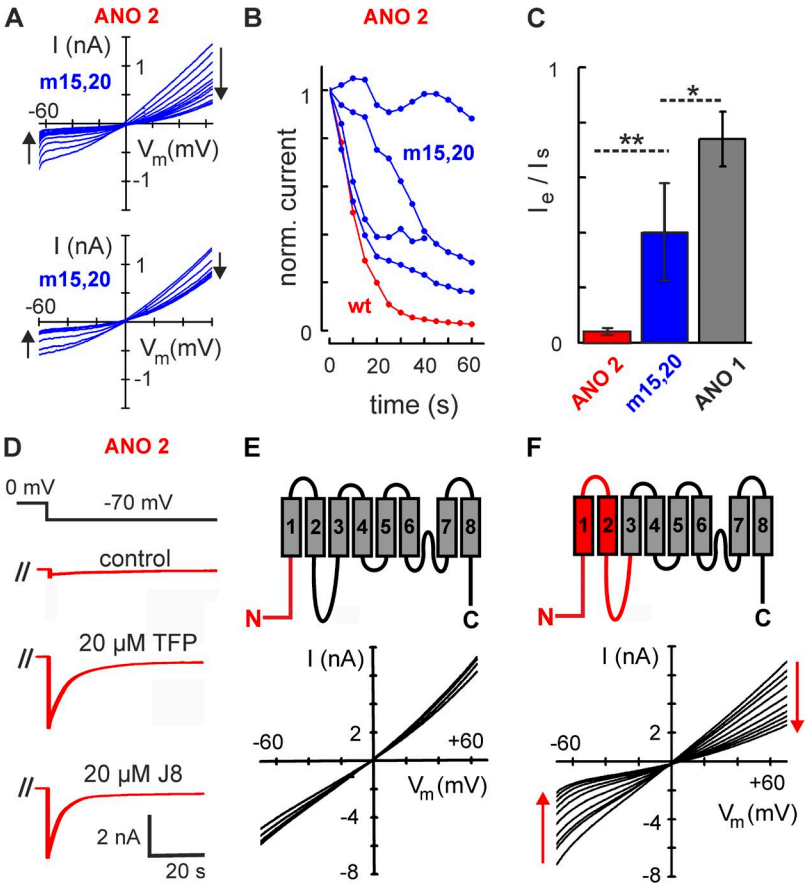

Figure 9. The distal section of the RCBM sequence contributes to inactivation of ANO 2 channels. (A) I/V relations recorded from 1-s voltage ramps at 5-s intervals display different speed and extent of current decline over 60 s in two cells expressing ANO 2 double mutants m15,20. (B) Four examples of current decline in ANO 2 channels with mutations in the distal segment. Inactivation kinetics exhibit large variability between individual cells. (C) The extent of inactivation, expressed as the ratio of the current amplitudes at the end (I_e) and at the start (I_s) of inactivation, differs strongly between wt ANO 2 and the ANO 2 mutant m15,20; the latter exhibits impaired inactivation. Mean I_e/I_s values are 0.039 ± 0.01 (n = 11) for ANO 2, 0.4 ± 0.18 (n = 6) for ANO 2 m15,20, and 0.74 ± 0.1 (n = 11) for ANO 1. **, $P < 0.01$; *, < 0.05; unpaired t test). Significance values were calculated for data connected by broken lines. Error bars indicate mean ± SEM. (D) Ca^{2+} preloading experiments (compare with Fig. 4 A) with 7.5 µM free Ca^{2+} at −70 mV show that inactivation of ANO 2 channels is suppressed by 20 µM TFP or 50 µM J-8, two CaM inhibitors, added to the bath solution. (E) ANO 1/ANO 2 chimaeras constructed to transfer inactivation to ANO 1. Integrating the N-terminal region of ANO 2 (red) into an ANO 1 background (gray) produced a functional but noninactivating channel, as demonstrated by the I/V_m curves recorded in 5-s intervals after the onset of the whole-cell configuration (bottom). (F) A chimera with an ANO 2 part extending from the N terminus to the position N515 of ANO 1 displayed inactivation with a time constant of 18.3 ± 3.1 s (3 cells) at −70 mV.

different sequence, we tested whether the ANO 2 N terminus supports inactivation when transferred onto an ANO 1 background. The resulting channel chimaera did not inactivate (I_e/I_s = 1.17 ± 0.32, 3 cells; Fig. 9 E). To transfer inactivation from ANO 2 to ANO 1, it was necessary to furnish the chimeric channel with the first two transmembrane domains of ANO 2, including their cytosolic appendages (Fig. 9 F). In this chimaera, the ANO 1 part starts with N515 at the cytoplasmic face of transmembrane region 3 (TMR3). This chimaera exhibited inactivation, similar in extent and speed to the ANO 2 wt channels. Thus, with the RCBM domain as an absolute requirement, the control of ANO channels is a function of an extended N-terminal module that encompasses the first two transmembrane regions.

Our search for additional domains that may control inactivation in this module was aided by a report on an ANO 2 channel cloned from the retina (Pifferi et al., 2009). In this study, current amplitudes did not decrease after a first measurement 30 s after whole-cell breakthrough. In fact, large ANO 2 currents could be recorded from ANO 2–expressing HEK 293 cells for up to 30 min. Thus, we subjected retinal ANO 2 channels to our inactivation protocol and confirmed that they did not inactivate (Fig. 10 A). A comparison of the primary structures of ANO 2 channels from OE and retina revealed that the retinal ANO 2 channel contained an additional stretch of four amino-acid residues (^{456}ERSQ) within the intracellular loop connecting transmembrane domains 2 and 3 (Fig. 10 B, segment *c*). Segment *c* is encoded by exon 15 of rat ANO 2 and is included in the retina-specific splice form of the channel (Stephan et al., 2009). Interestingly, the homologous region in ANO 1 (^{528}EAVK; Fig. 10 B) was shown to influence the Ca^{2+} sensitivity of the channel (Ferrera et al., 2009, 2011). Although it is not a Ca^{2+}-binding site itself, the motif appears to promote Ca^{2+} binding and to stabilize the open state (Xiao et al., 2011). The term "segment *c*" was coined for the region encoded by the human exon 13 and is commonly used in the ANO 1 literature (Ferrera et al., 2009). Our data show that segment *c* serves as a structural switch that suppresses channel inactivation in ANO 2, such that the absence of segment *c* is a necessary precondition for inactivation.

These results demonstrate a fundamental functional difference between the neuronal Ca^{2+}-activated Cl^- channel ANO 2 and the ubiquitous ANO 1 channel. ANO 2 can be expressed as a splice variant with intrinsic, Ca^{2+}-dependent inactivation, a property that may serve to support phasic, Ca^{2+}-dependent signaling in ANO 2–expressing neurons. To find out which splice variants of ANO 2 are expressed in the brain, we designed PCR primers that report the presence or absence of the exon encoding segment *c* in the ANO 2 mRNA. We found that the noninactivating splice form (with ^{456}ERSQ) was expressed in the retina and in the pineal organ. In contrast, the inactivating splice variant (without ^{456}ERSQ) was the major ANO 2 form expressed in cortex, hippocampus, cerebellum, and brain stem, as well as in the OE (Fig. 10 C). Thus, ANO 2 appears to

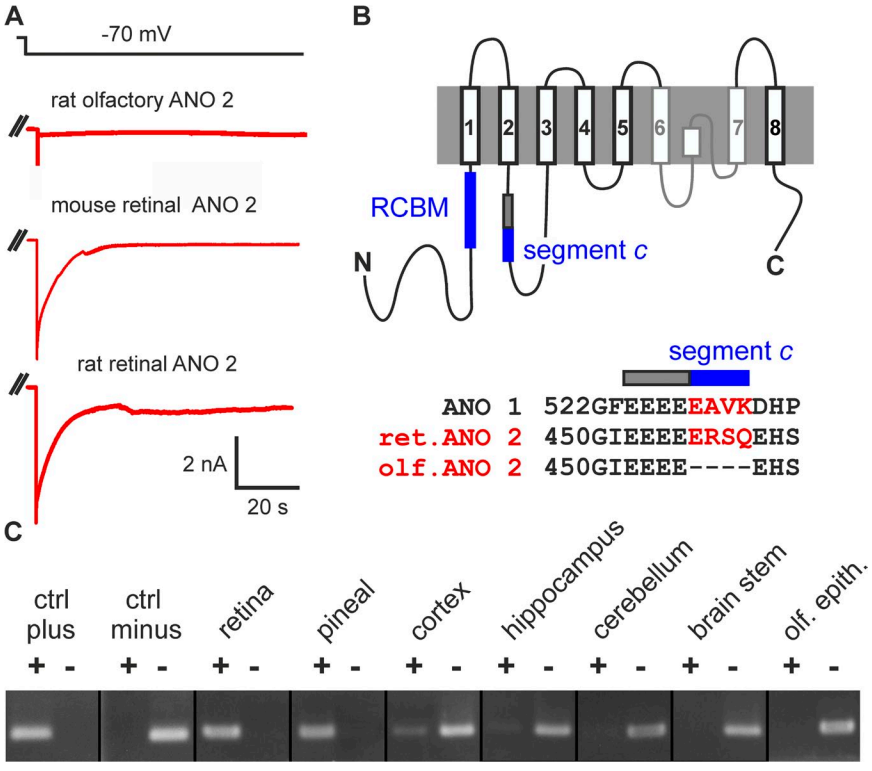

Figure 10. Inactivating and noninactivating splice variants of ANO 2 channels. (A) After preloading with 7.5 µM Ca^{2+} at 0 mV, the mouse olfactory ANO 2 channel displayed complete inactivation upon a voltage step to −70 mV (top trace). In contrast, the retinal splice variants in mouse and rat do not inactivate under identical conditions (bottom traces). (B) Topology model for ANO channels depicting the position of segment *c*. The alignment below illustrates that the four residues (in red) that constitute segment *c* are present in ANO 1 channels and in the retinal (ret.) splice variant of ANO 2 channels, but are not present in the olfactory (olf.) splice variant of ANO 2 channel. (C) RT-PCR analysis of the distribution of ANO 2 channel with and without segment *c*. Primers were designed to report the presence (+) or absence (−) of the respective exon (exon 13 in human ANO 1), and control RT-PCRs are shown with the retinal (ctrl plus) or olfactory (ctrl minus) variants of ANO 2. Tests with cDNA from various neuronal tissues revealed that the splice variant lacking segment ***c*** is expressed in most brain regions, whereas ANO 2 channels with segment ***c*** are restricted to the retina and the pineal organ.

be mostly used by the nervous system in its inactivating form. The noninactivating splice variant seems to serve a special function in vision and circadian regulation.

The RCBM sequence and segment *c* in the family of ANO proteins

As both the RCBM domain and segment *c* are clearly related to channel function, we compared them to the homologous sequences in ANO 3–10. Apparently, only one of these proteins can form ion channels: ANO 6 (alias TMEM16F), which was reported to encode nonselective cation channels (Yang et al., 2012). ANO 6 was also associated with Ca^{2+}-dependent anion conductance in various cell types (Martins et al., 2011; Szteyn et al., 2012; Tian et al., 2012; Grubb et al., 2013; Kunzelmann et al., 2013; Shimizu et al., 2013). For the other ANO proteins, channel activity has not yet been proven (Duran and Hartzell, 2011; Kunzelmann et al., 2011; Duran et al., 2012). Several residues in the corresponding regions are conserved throughout the 10 members of the ANO family, including the hydrophobic pair L323 and W327 in ANO 1 (Fig. 11 A). However, there are two striking differences: for ANO 1 and ANO 2 only, the RCBM sequence is encoded by a separate exon and recognized as a CRS motif. ANO 5 displays a slightly shifted CRS motif, whereas all other homologues have none at all. A comparison of RCBM sequences between the ANO proteins of rat and zebrafish shows a close similarity between fish and mammal, including the exon borders in ANO 1 and ANO 2 (Fig. 11 B; alignment in Fig. S1). Comparison of the regions homologous to segment *c* in ANO 1 and ANO 2 showed that none of the other eight ANOs possesses a similar motif (Fig. 11 C; alignment in Fig. S1). Furthermore, in the zebrafish ANO genes, the segment *c*–encoding sequences EAVK and ERSQ could not be identified in ANO 1 and ANO 2, and a conspicuous EEEE motif was present in ANO 2, but not in ANO 1 (Fig. S1). Thus, the RCBM functions as the proteins' interface with CaM and represents a regulatory structure in ANO channels in mammals and probably also in fish. Segment *c*, in turn, appears to be a modulatory structure in mammalian channels that promotes the stability of the channel's open state (Xiao et al., 2011).

In summary, our results indicate that the RCBM domain is a potentially bifunctional CaM-binding site.

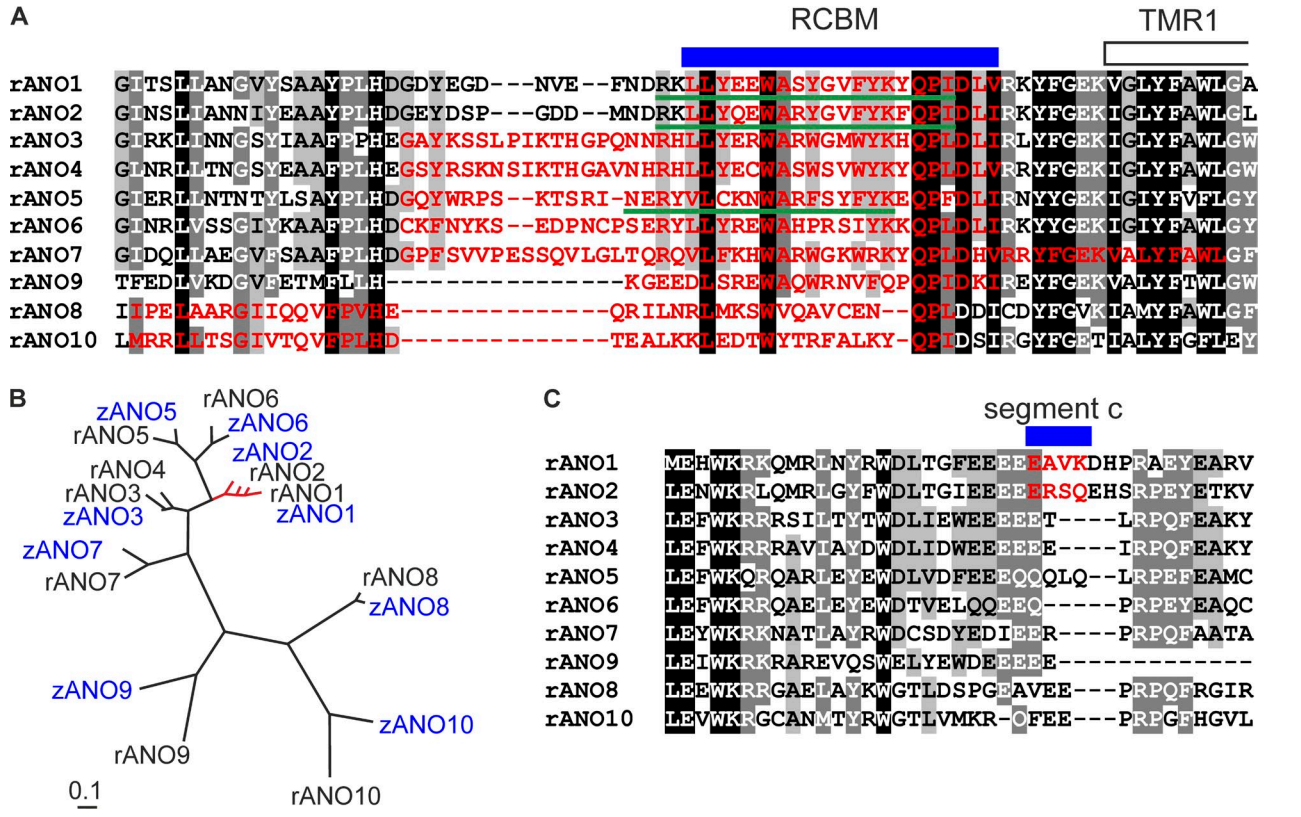

Figure 11. The RCBM sequence, segment *c*, and the homologous regions in the ANO family. (A) Alignment of the distal part of the N-terminal region for the ANO protein family in rat (r). The blue bar marks the RCBM sequence in ANO 1 and ANO 2. Regions encoded by the local exons are printed in red, the RCBM sequence is underlined in green. Percent identity: black = 100%; dark gray = 80%; light gray = 60%. (B) Phylogenetic tree of rat and zebrafish (z) ANO RCBM sequences illustrates a close similarity between the ion channel forming homologues ANO 1 and ANO 2 of fish and mammals. (C) Sequence alignment of the ANO region surrounding segment *c* in ANO 1 and ANO 2 illustrates the absence of that segment in ANO 3–10.

Although direct interaction between the RCBM domain and CaM has not yet been demonstrated in vivo, our data support the hypothesis that the RCBM domain promotes the Ca^{2+}-dependent activation process of ANO 1 and ANO 2 as examined in our recording protocol. In ANO 2, the RCBM domain also appears to promote inactivation, possibly through a second CaM molecule that binds at elevated Ca^{2+} concentrations. Full inactivation occurs only in ANO 2 channels, and it is prevented in splice variants that express segment *c*.

DISCUSSION

Since the discovery of ANO Ca^{2+}-activated Cl^- channels in 2008 (Caputo et al., 2008; Schroeder et al., 2008; Yang et al., 2008), the search for their activation mechanism was focused mainly on the most N-terminal section of the protein and on the intracellular loop connecting the second and third transmembrane regions. These parts of the protein attracted attention because they contain four alternatively spliced segments that have been first identified in human ANO 1 cDNA (Ferrera et al., 2009). One segment at the very N terminus is omitted when an alternative initiation site is used (segment *a*), and two alternatively spliced exons are located in the N-terminal region (exon 6b, segment *b*) and in the first intracellular loop (exon 13 coding for segment *c* and exon 15 coding for segment *d*). All of these segments influence the channels' sensitivity to Ca^{2+} and to membrane voltage. Moreover, it was recently discovered that ANO 2 in olfactory receptor neurons exists in two isoforms, each occurring in two distinct splice variants (Ponissery Saidu et al., 2013). Differences in Ca^{2+} sensitivity were discovered both between the isoforms and between the splice variants. Outside the N terminus, the first intracellular loop contains a conspicuous cluster of four glutamate residues, contiguous to segment *c*, the region encoded by exon 13 in human ANO 1. Initially a promising candidate for direct Ca^{2+} binding, this domain was later found to be dispensable for channel activation by Ca^{2+}. Instead, the EEEE stretch contributes to the voltage dependence of gating (Xiao et al., 2011; Cenedese et al., 2012). Recently, two glutamate residues in the third intracellular loop, positioned near the inner entrance of the channel pore (E702, E705), were shown to be critical for setting the Ca^{2+} sensitivity of ANO 1 (Yu et al., 2012). When these residues were replaced with uncharged glutamines, much higher Ca^{2+} concentrations were needed to open the channels. The EC_{50} for channel activation, measured in inside-out patches, increased to 70–2,000 µM Ca^{2+} in the point mutations. This extensive desensitization revealed that the respective protein region, the intracellular face of the pore structure, plays a key role in channel gating. Ca^{2+} binding to this region may be the rate-limiting step in the allosteric process that opens the channel. To prove this, it would be necessary to simultaneously record ligand binding and channel gating, which is difficult but possible (Biskup et al., 2007). At present, the channel region that contains E702 and E705 (^{702}EYMEM in ANO 1) is the most plausible candidate for a site of direct Ca^{2+} binding to ANO 1 and ANO 2 channels (Yu et al., 2012). This notion was supported by an examination of ANO1/ANO 2 chimaeras aimed at explaining the structural basis of different Ca^{2+} sensitivities in the two channels (Scudieri et al., 2013). The protein segment that connects TMR6 and TMR7, an intracellular section that contains the pore region and the two glutamates E702 and E705 (LOOP3 in Scudieri et al., 2013) was transferred from ANO 2 to ANO 1, and conferred to the chimaera the lower Ca^{2+} sensitivity typical of ANO 2. The same region was recently proposed to determine the density of ANO channels in the plasma membrane (Adomaviciene et al., 2013). Collectively, the studies available today indicate that the process leading from Ca^{2+} binding to channel opening involves several protein domains, and it is still difficult to assign distinct gating functions to protein domains in ANO channels. In the present study, we have identified an RCBM domain within the N-terminal region of the protein, a domain that appears to contribute to various functional aspects of these channels. The presence and the integrity of this domain are necessary for the virtually exclusive plasma-membrane localization of ANO 1 in HEK 293 cells. This observation does not, however, indicate that the RCBM domain contains any kind of membrane targeting signal. A more likely explanation is that the stability of the ANO 1 protein, which is extraordinary high in the wt protein (Tran et al., 2013), is reduced in the RCBM mutant. This may induce increased translational activity and, hence, increased immunolabeling of the ANO 1 mutants in intracellular membrane systems. The mutations do not prevent the mutant channels from inserting into the plasma membrane, as we have demonstrated for both Ca^{2+}-sensitive mutants (m11,15 of ANO 1 and ANO 2) and Ca^{2+}-insensitive mutants (m2 and m6 of ANO 1 and ANO 2). With respect to channel gating, our data provide strong evidence for the hypothesis that the intact RCBM domain is needed for Ca^{2+}-dependent activation of ANO 1 and ANO 2, as well as for Ca^{2+}-dependent inactivation of ANO 2.

Our data do not demonstrate that CaM binds to the RCBM domain in vivo, nor do they demonstrate that CaM does not bind to any RCBM mutation in vivo. This point is beyond the scope of the present study and has to be addressed with different methods in the future. Förster resonance energy transfer (FRET) between fluorescent protein tags attached to the RCBM domain and CaM is a suitable approach. CaM target domains were identified with FRET experiments in various ion channels, including L-type Ca^{2+} channels (Erickson et al.,

2001, 2003), cyclic nucleotide-gated channels (Trudeau and Zagotta, 2004), TRP channels (Derler et al., 2006), voltage-gated Na^+ channels (Biswas et al., 2008), and ryanodine receptor channels (Guo et al., 2011). In contrast, affinity tests based on CaM coprecipitation are less applicable here because, in addition to the RCBM domain, three other CaM-binding domains appear to be present (CAMBD1, CAMBD2, and CBM1; see "Interactions of the RCBM domain with Ca^{2+}/CaM") and may coprecipitate CaM. So far, our results introduce an additional candidate for a CaM target in ANO 1 and ANO 2, identified on the basis of in vitro binding assays with RCBM peptides and the channels' response to RCBM mutations.

Nonstationary analysis of ANO current

The rationale of our study was to examine the Ca^{2+}-induced activation of ANO 1 and ANO 2 inside the cell, under controlled ionic conditions, and before the onset of regulatory effects that might obscure the activation process. By comparing the functional properties of ANO 1 and ANO 2, we tried to identify special features that would qualify the neuronal channel ANO 2 for its functions in the nervous system. We focused on the channel activity within the first minute after contact with Ca^{2+}. Using pipette Ca^{2+} levels well in excess of the saturating concentrations for ANO 1 (>1 µM; Ferrera et al., 2009) and ANO 2 (>10 µM; Pifferi et al., 2009; Stephan et al., 2009), we ensured channel activation within 1–3 s after whole-cell breakthrough. This method was designed to produce steadily rising and eventually stable Ca^{2+} levels over the first minute of activation. Alternative methods were excluded because of the requirement for both fast and stable Ca^{2+} application. Photorelease from caged Ca^{2+} is much faster, but it is difficult to achieve a stable Ca^{2+} level over 60 s (Boccaccio and Menini, 2007; Boccaccio et al., 2011). Cellular Ca^{2+} signals that were either too slow or too transient for our purpose were induced by Ca^{2+} loading through ionomycin (Caputo et al., 2008), by opening of Ca^{2+}-permeable ion channels (Dzeja et al., 1999), or by the activation of phospholipase C—coupled receptors (Yang et al., 2008). Working with excised patches was ruled out because ANO channels change properties immediately upon excision, a "run-down" phenomenon that has been characterized in detail elsewhere (Reisert et al., 2003; Kaneko et al., 2006; Pifferi et al., 2009; Ponissery Saidu et al., 2013). Nonstationary current analysis during cell perfusion with Ca^{2+} produced highly reproducible data in several hundred recordings. These data could be used in experiments with site-directed mutagenesis and pharmacological intervention. A drawback of this method is that the reversibility of cellular processes cannot be examined systematically because Ca^{2+} cannot be removed from the cell once the whole-cell configuration is established. Also, the nonstationary current signals had to be carefully analyzed, as they consisted of three distinct components: channel activation, Cl^- depletion, and channel inactivation. Cl^- depletion is the combined consequence of the large Cl^- efflux in our experiments and the relatively low Cl^- affinity of Ca^{2+}-activated Cl^- channels (the K_D for Cl^- is 73 mM in *Xenopus laevis* oocyte channels; Qu and Hartzell, 2000). Thus, a decrease of Cl^- current already occurs at relatively high Cl^- concentrations, when intracellular Cl^- drops below the K_D value of the channels. We could not determine precisely how far the Cl^- levels decreased during channel activation because measurements of E_{Cl} through analysis of I/V_m relations always admitted Cl^- influx into the cell and hence raised the Cl^- concentration. But the I/V_m analysis provided a rough estimate: the lowest Cl^- concentration upon depletion must be below 30–50 mM because these concentrations were estimated from E_{Cl} recordings after partial recovery of the Cl^- level. Depletion is a critical aspect especially of ANO 2 physiology, because this channel seems to be located exclusively in cell compartments with very small volume like cilia (Stephan et al., 2009; Hengl et al., 2010; Dauner et al., 2012), dendrites (Huang et al., 2012c), and presynaptic terminals (Dauner et al., 2013). Activation of these channels is therefore expected to change the intracellular Cl^- levels efficiently, as was analyzed quantitatively for olfactory cilia (Lindemann, 2001). Collectively, the nonstationary analysis of ANO 1 and ANO 2 currents provided functional information within an early time window of channel activity in the whole-cell configuration.

Interactions of the RCBM domain with Ca^{2+}/CaM

The RCBM sequence is encoded by a separate exon (exon 9 in human ANO 1), which is conserved in the ANO genomic structure from fish to mammals. The amino-acid sequence is recognized as a CRS motif by the Calmodulin Target Database (Yap et al., 2000) specifically in ANO 1 and ANO 2, as well as in ANO 5. The RCBM domain does not correspond to three previously proposed CaM-binding sites in ANO 1, all of which have been shown to be unnecessary for channel activation (CAMBD1 and CAMBD2 in Tian et al. [2011] and CBM2 in Jung et al. [2013]). CAMBD1 could be deleted without loss of channel function (Ferrera et al., 2009). CAMBD2 shows an overlap with the distal part of the RCBM domain. However, it was not classified as a CRS motif in our bioinformatic analysis, as it reached into the first transmembrane region (which, in our analysis, starts at ^{350}V in ANO 1; Fig. 5 C). A peptide corresponding to the CAMBD2 sequence was not able to counteract channel activation (Tian et al., 2011), which may indicate that this sequence does not bind CaM. However, an I-to-A exchange in the position corresponding to ^{339}I of our sequence (Fig. 5 C) did reduce CaM binding to the ANO 1 protein (Jung et al., 2013). This finding may be explained by a compromised association of

CaM with the RCBM sequence, as ^{339}I is part of the distal section of RCBM. Finally, channels with mutations in the CBM2 domain were functional but displayed slightly reduced bicarbonate permeability (Jung et al., 2013). Thus, the three previously characterized CaM-binding motifs did not display the crucial significance for channel activation that we found for the RCBM domain, inasmuch that the channels tolerate mutations in these sequences, but not in RCBM.

Our peptide studies demonstrated that CaM binding to the RCBM is Ca^{2+} dependent, but requires only submicromolar Ca^{2+} concentrations. Moreover, the binding assays suggest that the RCBM harbors two distinct sites of interaction, one high-affinity site in the proximal section, and one low-affinity site in the distal section. This finding suggests that the RCBM may be able to process two distinct CaM-mediated signals. Structurally, the RCBM resembles the CaM-binding site of skeletal myosin light-chain kinase (Peersen et al., 1997). This site is also characterized by flanking pairs of basic residues, and it binds CaM at similar Ca^{2+} concentrations as the high-affinity site on the RCBM peptide. However, although the basic residues encase a stretch of 14 amino acids in the myosin light-chain kinase motif, the RCBM has 21 amino acids inside its RK–RK bracket. The RCBM motif may contain two α-helical regions, which appear to provide the structural basis of the two interaction sites. However, whether the RCBM sequence can bind one or two CaM molecules has not yet been established. The stoichiometry has to be examined by analytical ultracentrifugation, fluorescence correlation spectroscopy, or NMR studies. So far, we conclude that the RCBM peptide binds Ca^{2+}/CaM at two distinct affinities, and that a single lobe of the CaM molecule is sufficient for high-affinity interaction.

The RCBM and channel activation

Mutations that perturb hydropathy within the proximal section of the RCBM render the channels nonfunctional. This finding may indicate that the binding of Ca^{2+}/CaM to the RCBM is a necessary step in channel activation. However, application of the CaM inhibitors TFP and J-8 did not block channel activation. In an earlier report, the two inhibitors indeed blocked the activation of ANO 1 in HEK 293 cells (Tian et al., 2011). In our experiments, both ANO 1 and ANO 2 activation were resistant to TFP and J-8 at the same concentrations. This discrepancy may be attributed to the different experimental protocols used. We monitored the rapid activation of Cl^- currents upon Ca^{2+} perfusion of cells, using CsCl solution on both sides of the membrane. In the earlier study, ionomycin was used to permeabilize the plasma membrane for Ca^{2+} ions, and physiological cation concentrations (K^+, Na^+) were applied. It appears that the rapid effects in our experiments are resistant to TFP and J-8, but that subsequent cellular processes, recorded under equilibrium conditions, can be inhibited. One clue resulting from our peptide studies is the strikingly high affinity of Ca^{2+}/CaM binding to the RCBM peptides. EC_{50} values of 0.1–0.2 µM Ca^{2+} are well below the concentrations required for half-maximal channel activation (ANO 1, ∼0.3 µM; ANO 2, ∼2 µM). Moreover, the observation that the CaM mutants CaM12 and CaM34 bind with almost the same affinity as wt CaM may suggest that the high-affinity association represents a stable binding of CaM to the RCBM at low Ca^{2+} concentrations. In this scenario, one lobe of CaM would be tethered to the RCBM at low Ca^{2+} concentrations without activating the channel. The other CaM lobe would bind Ca^{2+} and induce channel opening when Ca^{2+} concentrations increase. Tethered CaM molecules can be inaccessible for TFP and J-8. A similar combination of high Ca^{2+} affinity and resistance against CaM inhibitors was shown for other ion channels that are gated by stably associated Ca^{2+}/CaM, in particular small-conductance, Ca^{2+} activated K^+ channels (SK, KCa2.3; Xia et al., 1998), intermediate-conductance Ca^{2+}-activated K^+ channels (IK_{Ca}, KCa3.1; Del Carlo et al., 2002), and cyclic nucleotide-gated channels (Bradley et al., 2001, 2004).

In contrast, channels that bind CaM in a Ca^{2+}-independent way are usually equipped with IQ-type CaM-binding sites (Bähler and Rhoads, 2002), and CaM effects can be antagonized with the Ca^{2+}-free mutant CaM1234 (DeMaria et al., 2001; Alseikhan et al., 2002; Mori et al., 2004; Halling et al., 2006; Kasri et al., 2006). Neither of these points applies to ANO channels, so Ca^{2+}-independent association with apo-CaM can be ruled out. Thus, although high-affinity binding, single-lobe association, and TFP/ J-8 resistance are consistent with a stable, Ca^{2+}-dependent association of CaM with ANO channels, critical information is still missing. Coprecipitation (Tian et al., 2011; Jung et al., 2013) does not provide information about the site of interaction. Moreover, ANO 1 and ANO 2 channels are expressed as homodimers (Fallah et al., 2011; Sheridan et al., 2011; Tien et al., 2013) or ANO 1/ANO 2 heterodimers, a subunit assembly that is governed by a dimerization domain located between the N terminus and the RCBM (Tien et al., 2013). Thus, the quaternary structure complicates the question of stoichiometry in the CaM–RCBM complex. Finally, the distinct difference in CaM-binding properties between the RCBM peptides from ANO 1 and ANO 2 requires further examination. In this context, other divalent cations may be helpful, in particular Ba^{2+}, which activates CaM at 200-fold higher concentrations than Ca^{2+} (Yamazaki et al., 1996; Kursula and Majava, 2007). Ba^{2+} (1 mM) was reported to activate ANO 1 (Xiao et al., 2011) but not ANO 2 (Reisert et al., 2003), and may help to further characterize CaM-binding to the RCBM.

The RCBM and ANO 2 inactivation

Our peptide assays and mutagenesis results indicate that the distal part of the RCBM is involved in Ca^{2+}-dependent inactivation of the neuron-specific ANO 2 channels. This inactivation is a relatively slow process, fully developing within 30 s under our experimental conditions. Inactivation appears to be reversible, does not depend on protein kinase activity, and can be blocked by the CaM inhibitors TFP and J-8. The kinetics of this inactivation process are probably diffusion-limited, reflecting the availability of Ca^{2+}/CaM in the cytosol and its association rate with the channel. Thus, the measured inactivation time constant of 12 s at −70 mV must be seen as the result of our recording situation. The speed of inactivation can be reduced by cell perfusion, by Ca^{2+} binding to 10 mM HEDTA in our pipette solution with its buffer capacity in the range of 0.5–5 µM Ca^{2+} (Durham, 1983), and by dilution of free cytosolic CaM in the whole-cell configuration. In intact neurons, particularly in dendritic or synaptic structures where ANO 2 channels are localized, inactivation may be significantly faster. An important finding is that inactivation is completely suppressed when ANO 2 channels express the four amino acids of segment *c*. This is in line with recent results on the function of segment *c* in ANO 1 gating. A biophysical examination of the mouse ANO 1 splice variant that contained segments *a* and *c* revealed that segment *c* stabilized the open state of the channel by increasing its apparent Ca^{2+} affinity (Xiao et al., 2011). It is conceivable that the same mode of operation counteracts channel inactivation in the retinal ANO 2 splice variant that possesses segment *c* (Stephan et al., 2009).

The sensitivity of ANO 2 inactivation to CaM inhibitors can be interpreted as indicative of a second CaM molecule that is not stably associated with ANO 2, but binds to the channel at elevated Ca^{2+} concentrations. Both TFP and J-8 prevent the Ca^{2+}-induced association of CaM with a protein (Craven et al., 1996; Feldkamp et al., 2010). The inhibitors antagonize Ca^{2+} effects by reducing the concentration of free CaM in the cell. Their blocking effect on ANO 2 inactivation seen in our experiments indicates that this process, in contrast to activation, depends on the availability of free CaM. Moreover, the observation that mutations in the distal section of the RCBM interfere with channel inactivation suggests that it is CaM-binding to this part of the RCBM that induces channel inactivation. Congruent with this interpretation is the finding that, in contrast to the ANO 1 peptide, the distal section of the ANO 2 peptide is not required for high-affinity binding. This points to a distinct function of the distal part in ANO 2, a function associated with the low-affinity binding of Ca^{2+}/CaM. This functional difference between ANO 1 and ANO 2 is remarkable considering that the sequences of the RCBM differ only in two positions (15 and 21). Thus, our results provide a consistent set of data that support the hypothesis that the RCBM of ANO 2 is not only involved in the activation process, but also in channel inactivation. However, our experiments with channel chimaera demonstrate that inactivation requires more than just the RCBM. Inactivation apparently is brought about by a larger region of the channel, encompassing the first two transmembrane domains and their connecting loop. Importantly, this region may also contain the four amino acids of segment *c*, encoded by a separate exon, which completely suppresses inactivation in the ANO 2 splice variant expressed in photoreceptors.

Inactivating and noninactivating forms of ANO 2

With respect to the inclusion of segment *c* and to its specific site of expression, the noninactivating retinal ANO 2 channel appears to be an exceptional case among neuronal ANO 2 channels. In retinal photoreceptors, Ca^{2+}-activated Cl^- channels are targeted to the presynaptic region of the photoreceptor terminals where they are proposed to partake in the regulation of presynaptic Ca^{2+} currents (Thoreson et al., 2003; Stöhr et al., 2009). The channels do not show pronounced inactivation and are thought to serve as a link in a feedback regulatory chain that limits transmitter release (Thoreson et al., 2000, 2002, 2003; Mercer et al., 2011). ANO 1 channels have been reported to be expressed in rod and cone terminals (Mercer et al., 2011; Jeon et al., 2013). We have recently found that ANO 2 is specifically expressed in rod terminals and absent from cone photoreceptors, which suggests a distinct role in the regulation of transmitter release under scotopic conditions (Dauner et al., 2013). In contrast to the photoreceptor channel, the inactivating ANO 2 splice variant without segment *c* is the most common one in various brain regions. Best examined so far are ANO 2 channels in the chemosensory neurons of the nose (Reisert et al., 2003; Hengl et al., 2010; Billig et al., 2011; Dauner et al., 2012; Dibattista et al., 2012) and in hippocampal pyramidal neurons (Huang et al., 2012c). In both cases, ANO 2 channels are expressed not in the axons, but in the dendritic and somatic regions of the neurons, and they are involved in translating incoming signals into excitation patterns. In chemosensory neurons, they are targeted to the chemosensory membrane at the distal end of the dendrite (Rasche et al., 2010; Dibattista et al., 2012) and are thought to amplify the receptor current and hence the detection efficiency of these sensory neurons (Reisert et al., 2005; Hengl et al., 2010; Kim et al., 2011). The response of olfactory receptor neurons is typically phasic, and the neurons show pronounced adaptation behavior (Ghatpande and Reisert, 2011). The underlying termination of receptor current is triggered by the removal of intracellular Ca^{2+} and, hence, by the deactivation of ANO 2 channels at decreasing Ca^{2+} concentrations. The potassium-dependent Na^+/Ca^{2+} exchanger NCKX4 extrudes Ca^{2+} and thereby determines the temporal

stimulus–response relation of these neurons (Stephan et al., 2011). With its Ca^{2+}-dependent inactivation, ANO 2 may aid in the termination of receptor current. Inactivation is suited to curtail the Cl^- component of the receptor current even before the Ca^{2+} concentration has returned to baseline levels. Thus, for the chemosensory neurons of the nose, our results suggest an enforcement of adaptive behavior through inactivation of ANO 2 channels.

In hippocampal pyramidal neurons, ANO 2 channels are opened when Ca^{2+} enters the dendrites through NMDA-type glutamate receptors. The resulting Ca^{2+}-induced Cl^- conductance reduces amplitude and summation of excitatory postsynaptic potentials (EPSP), and decreases action potential duration and EPSP–spike coupling (Huang et al., 2012c). Thus, in contrast to its excitatory role in chemosensory neurons, ANO 2 in the hippocampus serves an inhibitory function. It reduces the efficiency by which EPSPs are translated into action potentials, thus modulating firing frequency and firing patterns. Moreover, by reducing action potential duration, it reduces the probability for temporal coincidence of spikes elicited by synaptic activity with back-propagated spikes that enter the dendrite from the soma (Caporale and Dan, 2008). In this way, ANO 2 currents may reduce signal potentiation in CA1 and CA3 pyramidal neurons in the hippocampus. These opposite effects of ANO 2 currents in chemosensory and in hippocampal neurons are the consequence of different regimes of Cl^- homeostasis in these neurons. Chemosensory neurons actively accumulate Cl^- at rest and, upon stimulation, discharge a depolarizing Cl^- efflux through Ca^{2+}-activated Cl^- channels (Kaneko et al., 2004; Yang and Delay, 2010). Hippocampal pyramidal neurons, in contrast, maintain low Cl^- levels, and hence, the driving force for Cl^- influx that stabilizes the resting membrane voltage (Payne et al., 2003). However, intracellular Cl^- concentrations can change in neurons, mainly due to the antagonistic regulation of the Cl^- transporters NKCC1 and KCC2 (Blaesse et al., 2009). Consequently, the impact of Ca^{2+}-activated Cl^- channels on neuronal excitation is codetermined by the prevailing intracellular Cl^- level under physiological and pathological conditions.

In conclusion, our nonstationary current analysis of ANO channels has led to the identification of an N-terminal domain that is involved in channel regulation by Ca^{2+}. The RCBM domain may serve as a high-affinity Ca^{2+}/CaM-binding domain involved in the activation in ANO 1 and ANO 2 channels. In addition, it may provide a second, low-affinity binding site that mediates the Ca^{2+}-dependent inactivation process in neuronal ANO 2 channels.

Online supplemental material

Fig. S1 shows alignments of rat and zebrafish ANO proteins. Table S1 shows the composition of pipette solutions. Table S2 shows primers used for cloning, RT-PCR analysis and mutagenesis. Online supplemental material is available at http://www.jgp.org/cgi/content/full/jgp.201311015/DC1.

This work was supported by the Deutsche Forschungsgemeinschaft (MO 1384/2-3).

Author contributions: K. Vocke performed the mutagenesis and electrophysiology; K. Dauner analyzed the ANO-2 splice variants; K. Dauner, A. Hahn, and A. Ulbrich performed the binding studies; J. Broecker and S. Keller performed the CD analysis. F. Möhrlen and S. Frings designed the project and wrote the manuscript.

Angus C. Nairn served as editor.

Submitted: 25 April 2013
Accepted: 26 August 2013

REFERENCES

Adomaviciene, A., K.J. Smith, H. Garnett, and P. Tammaro. 2013. Putative pore-loops of TMEM16/anoctamin channels affect channel density in cell membranes. *J. Physiol.* 591:3487–3505. http://dx.doi.org/10.1113/jphysiol.2013.251660

Alseikhan, B.A., C.D. DeMaria, H.M. Colecraft, and D.T. Yue. 2002. Engineered calmodulins reveal the unexpected eminence of Ca2+ channel inactivation in controlling heart excitation. *Proc. Natl. Acad. Sci. USA.* 99:17185–17190. http://dx.doi.org/10.1073/pnas.262372999

Angermann, J.E., A.R. Sanguinetti, J.L. Kenyon, N. Leblanc, and I.A. Greenwood. 2006. Mechanism of the inhibition of Ca^{2+}-activated Cl^- currents by phosphorylation in pulmonary arterial smooth muscle cells. *J. Gen. Physiol.* 128:73–87. http://dx.doi.org/10.1085/jgp.200609507

Ayon, R., W. Sones, A.S. Forrest, M. Wiwchar, M.L. Valencik, A.R. Sanguinetti, B.A. Perrino, I.A. Greenwood, and N. Leblanc. 2009. Complex phosphatase regulation of Ca2+-activated Cl^- currents in pulmonary arterial smooth muscle cells. *J. Biol. Chem.* 284:32507–32521. http://dx.doi.org/10.1074/jbc.M109.050401

Bähler, M., and A. Rhoads. 2002. Calmodulin signaling via the IQ motif. *FEBS Lett.* 513:107–113. http://dx.doi.org/10.1016/S0014-5793(01)03239-2

Berg, J., H. Yang, and L.Y. Jan. 2012. Ca2+-activated Cl^- channels at a glance. *J. Cell Sci.* 125:1367–1371. http://dx.doi.org/10.1242/jcs.093260

Billig, G.M., B. Pál, P. Fidzinski, and T.J. Jentsch. 2011. Ca2+-activated Cl^- currents are dispensable for olfaction. *Nat. Neurosci.* 14:763–769. http://dx.doi.org/10.1038/nn.2821

Biskup, C., J. Kusch, E. Schulz, V. Nache, F. Schwede, F. Lehmann, V. Hagen, and K. Benndorf. 2007. Relating ligand binding to activation gating in CNGA2 channels. *Nature.* 446:440–443. http://dx.doi.org/10.1038/nature05596

Biswas, S., I. Deschênes, D. Disilvestre, Y. Tian, V.L. Halperin, and G.F. Tomaselli. 2008. Calmodulin regulation of Nav1.4 current: role of binding to the carboxyl terminus. *J. Gen. Physiol.* 131:197–209. http://dx.doi.org/10.1085/jgp.200709863

Blaesse, P., M.S. Airaksinen, C. Rivera, and K. Kaila. 2009. Cation-chloride cotransporters and neuronal function. *Neuron.* 61:820–838. http://dx.doi.org/10.1016/j.neuron.2009.03.003

Boccaccio, A., and A. Menini. 2007. Temporal development of cyclic nucleotide-gated and Ca2+ -activated Cl^- currents in isolated mouse olfactory sensory neurons. *J. Neurophysiol.* 98:153–160. http://dx.doi.org/10.1152/jn.00270.2007

Boccaccio, A., C. Sagheddu, and A. Menini. 2011. Flash photolysis of caged compounds in the cilia of olfactory sensory neurons. *J. Vis. Exp.* e3195. http://dx.doi.org/10.3791/3195

Bradley, J., D. Reuter, and S. Frings. 2001. Facilitation of calmodulin-mediated odor adaptation by cAMP-gated channel subunits. *Science.* 294:2176–2178. http://dx.doi.org/10.1126/science.1063415

Bradley, J., W. Bönigk, K.W. Yau, and S. Frings. 2004. Calmodulin permanently associates with rat olfactory CNG channels under native conditions. *Nat. Neurosci.* 7:705–710. http://dx.doi.org/10.1038/nn1266

Caporale, N., and Y. Dan. 2008. Spike timing-dependent plasticity: a Hebbian learning rule. *Annu. Rev. Neurosci.* 31:25–46. http://dx.doi.org/10.1146/annurev.neuro.31.060407.125639

Caputo, A., E. Caci, L. Ferrera, N. Pedemonte, C. Barsanti, E. Sondo, U. Pfeffer, R. Ravazzolo, O. Zegarra-Moran, and L.J.V. Galietta. 2008. TMEM16A, a membrane protein associated with calcium-dependent chloride channel activity. *Science.* 322:590–594. http://dx.doi.org/10.1126/science.1163518

Cenedese, V., G. Betto, F. Celsi, O.L. Cherian, S. Pifferi, and A. Menini. 2012. The voltage dependence of the TMEM16B/anoctamin2 calcium-activated chloride channel is modified by mutations in the first putative intracellular loop. *J. Gen. Physiol.* 139:285–294. http://dx.doi.org/10.1085/jgp.201110764

Cho, H., Y.D. Yang, J. Lee, B. Lee, T. Kim, Y. Jang, S.K. Back, H.S. Na, B.D. Harfe, F. Wang, et al. 2012. The calcium-activated chloride channel anoctamin 1 acts as a heat sensor in nociceptive neurons. *Nat. Neurosci.* 15:1015–1021. http://dx.doi.org/10.1038/nn.3111

Craven, C.J., B. Whitehead, S.K. Jones, E. Thulin, G.M. Blackburn, and J.P. Waltho. 1996. Complexes formed between calmodulin and the antagonists J-8 and TFP in solution. *Biochemistry.* 35:10287–10299. http://dx.doi.org/10.1021/bi9605043

Dauner, K., J. Lissmann, S. Jeridi, S. Frings, and F. Möhrlen. 2012. Expression patterns of anoctamin 1 and anoctamin 2 chloride channels in the mammalian nose. *Cell Tissue Res.* 347:327–341. http://dx.doi.org/10.1007/s00441-012-1324-9

Dauner, K., C. Möbus, S. Frings, and F. Möhrlen. 2013. Targeted expression of anoctamin calcium-activated chloride channels in rod photoreceptor terminals of the rodent retina. *Invest. Ophthalmol. Vis. Sci.* 54:3126–3136. http://dx.doi.org/10.1167/iovs.13-11711

Davis, A.J., A.S. Forrest, T.A. Jepps, M.L. Valencik, M. Wiwchar, C.A. Singer, W.R. Sones, I.A. Greenwood, and N. Leblanc. 2010. Expression profile and protein translation of TMEM16A in murine smooth muscle. *Am. J. Physiol. Cell Physiol.* 299:C948–C959. http://dx.doi.org/10.1152/ajpcell.00018.2010

Del Carlo, B., M. Pellegrini, and M. Pellegrino. 2002. Calmodulin antagonists do not inhibit IK(Ca) channels of human erythrocytes. *Biochim. Biophys. Acta.* 1558:133–141. http://dx.doi.org/10.1016/S0005-2736(01)00419-9

DeMaria, C.D., T.W. Soong, B.A. Alseikhan, R.S. Alvania, and D.T. Yue. 2001. Calmodulin bifurcates the local Ca2+ signal that modulates P/Q-type Ca2+ channels. *Nature.* 411:484–489. http://dx.doi.org/10.1038/35078091

Derler, I., M. Hofbauer, H. Kahr, R. Fritsch, M. Muik, K. Kepplinger, M.E. Hack, S. Moritz, R. Schindl, K. Groschner, and C. Romanin. 2006. Dynamic but not constitutive association of calmodulin with rat TRPV6 channels enables fine tuning of Ca2+-dependent inactivation. *J. Physiol.* 577:31–44. http://dx.doi.org/10.1113/jphysiol.2006.118661

Dibattista, M., A. Amjad, D.K. Maurya, C. Sagheddu, G. Montani, R. Tirindelli, and A. Menini. 2012. Calcium-activated chloride channels in the apical region of mouse vomeronasal sensory neurons. *J. Gen. Physiol.* 140:3–15. http://dx.doi.org/10.1085/jgp.201210780

Dick, I.E., M.R. Tadross, H. Liang, L.H. Tay, W. Yang, and D.T. Yue. 2008. A modular switch for spatial Ca2+ selectivity in the calmodulin regulation of CaV channels. *Nature.* 451:830–834. http://dx.doi.org/10.1038/nature06529

Duran, C., and H.C. Hartzell. 2011. Physiological roles and diseases of Tmem16/Anoctamin proteins: are they all chloride channels? *Acta Pharmacol. Sin.* 32:685–692. http://dx.doi.org/10.1038/aps.2011.48

Duran, C., Z. Qu, A.O. Osunkoya, Y. Cui, and H.C. Hartzell. 2012. ANOs 3-7 in the anoctamin/Tmem16 Cl^- channel family are intracellular proteins. *Am. J. Physiol. Cell Physiol.* 302:C482–C493. http://dx.doi.org/10.1152/ajpcell.00140.2011

Durham, A.C. 1983. A survey of readily available chelators for buffering calcium ion concentrations in physiological solutions. *Cell Calcium.*4:33–46.http://dx.doi.org/10.1016/0143-4160(83)90047-7

Dzeja, C., V. Hagen, U.B. Kaupp, and S. Frings. 1999. Ca2+ permeation in cyclic nucleotide-gated channels. *EMBO J.* 18:131–144. http://dx.doi.org/10.1093/emboj/18.1.131

Erickson, M.G., B.A. Alseikhan, B.Z. Peterson, and D.T. Yue. 2001. Preassociation of calmodulin with voltage-gated Ca(2+) channels revealed by FRET in single living cells. *Neuron.* 31:973–985. http://dx.doi.org/10.1016/S0896-6273(01)00438-X

Erickson, M.G., H. Liang, M.X. Mori, and D.T. Yue. 2003. FRET two-hybrid mapping reveals function and location of L-type Ca2+ channel CaM preassociation. *Neuron.* 39:97–107. http://dx.doi.org/10.1016/S0896-6273(03)00395-7

Fallah, G., T. Römer, S. Detro-Dassen, U. Braam, F. Markwardt, and G. Schmalzing. 2011. TMEM16A(a)/anoctamin-1 shares a homodimeric architecture with CLC chloride channels. *Mol. Cell. Proteomics.* 10:M110.004697.

Feldkamp, M.D., S.E. O'Donnell, L. Yu, and M.A. Shea. 2010. Allosteric effects of the antipsychotic drug trifluoperazine on the energetics of calcium binding by calmodulin. *Proteins.* 78:2265–2282. http://dx.doi.org/10.1002/prot.22739

Ferrera, L., A. Caputo, I. Ubby, E. Bussani, O. Zegarra-Moran, R. Ravazzolo, F. Pagani, and L.J.V. Galietta. 2009. Regulation of TMEM16A chloride channel properties by alternative splicing. *J. Biol. Chem.* 284:33360–33368. http://dx.doi.org/10.1074/jbc.M109.046607

Ferrera, L., P. Scudieri, E. Sondo, A. Caputo, E. Caci, O. Zegarra-Moran, R. Ravazzolo, and L.J.V. Galietta. 2011. A minimal isoform of the TMEM16A protein associated with chloride channel activity. *Biochim. Biophys. Acta.* 1808:2214–2223. http://dx.doi.org/10.1016/j.bbamem.2011.05.017

Gangopadhyay, J.P., Z. Grabarek, and N. Ikemoto. 2004. Fluorescence probe study of Ca2+-dependent interactions of calmodulin with calmodulin-binding peptides of the ryanodine receptor. *Biochem. Biophys. Res. Commun.* 323:760–768. http://dx.doi.org/10.1016/j.bbrc.2004.08.154

Ghatpande, A.S., and J. Reisert. 2011. Olfactory receptor neuron responses coding for rapid odour sampling. *J. Physiol.* 589:2261–2273. http://dx.doi.org/10.1113/jphysiol.2010.203687

Grubb, S., K.A. Poulsen, C.A. Juul, T. Kyed, T.K. Klausen, E.H. Larsen, and E.K. Hoffmann. 2013. TMEM16F (Anoctamin 6), an anion channel of delayed Ca(2+) activation. *J. Gen. Physiol.* 141:585–600. http://dx.doi.org/10.1085/jgp.201210861

Guo, T., B.R. Fruen, F.R. Nitu, T.D. Nguyen, Y. Yang, R.L. Cornea, and D.M. Bers. 2011. FRET detection of calmodulin binding to the cardiac RyR2 calcium release channel. *Biophys. J.* 101:2170–2177. http://dx.doi.org/10.1016/j.bpj.2011.09.030

Halling, D.B., P. Aracena-Parks, and S.L. Hamilton. 2006. Regulation of voltage-gated Ca2+ channels by calmodulin. *Sci. STKE.* 2006:er1.

Hartzell, C., I. Putzier, and J. Arreola. 2005. Calcium-activated chloride channels. *Annu. Rev. Physiol.* 67:719–758. http://dx.doi.org/10.1146/annurev.physiol.67.032003.154341

Hartzell, H.C., K. Yu, Q. Xiao, L.T. Chien, and Z. Qu. 2009. Anoctamin/TMEM16 family members are Ca2+-activated Cl^- channels. *J. Physiol.* 587:2127–2139. http://dx.doi.org/10.1113/jphysiol.2008.163709

Hengl, T., H. Kaneko, K. Dauner, K. Vocke, S. Frings, and F. Möhrlen. 2010. Molecular components of signal amplification in olfactory sensory cilia. *Proc. Natl. Acad. Sci. USA.* 107:6052–6057. http://dx.doi.org/10.1073/pnas.0909032107

Huang, F., J.R. Rock, B.D. Harfe, T. Cheng, X.Z. Huang, Y.N. Jan, and L.Y. Jan. 2009. Studies on expression and function of the TMEM16A calcium-activated chloride channel. *Proc. Natl. Acad. Sci. USA.* 106:21413–21418. http://dx.doi.org/10.1073/pnas.0911935106

Huang, F., X. Wong, and L.Y. Jan. 2012a. International Union of Basic and Clinical Pharmacology. LXXXV: calcium-activated chloride channels. *Pharmacol. Rev.* 64:1–15. http://dx.doi.org/10.1124/pr.111.005009

Huang, F., H. Zhang, M. Wu, H. Yang, M. Kudo, C.J. Peters, P.G. Woodruff, O.D. Solberg, M.L. Donne, X. Huang, et al. 2012b. Calcium-activated chloride channel TMEM16A modulates mucin secretion and airway smooth muscle contraction. *Proc. Natl. Acad. Sci. USA.* 109:16354–16359. http://dx.doi.org/10.1073/pnas.1214596109

Huang, W.C., S. Xiao, F. Huang, B.D. Harfe, Y.N. Jan, and L.Y. Jan. 2012c. Calcium-activated chloride channels (CaCCs) regulate action potential and synaptic response in hippocampal neurons. *Neuron.* 74:179–192. http://dx.doi.org/10.1016/j.neuron.2012.01.033

Huelsenbeck, J.P., and F. Ronquist. 2001. MRBAYES: Bayesian inference of phylogenetic trees. *Bioinformatics.* 17:754–755. http://dx.doi.org/10.1093/bioinformatics/17.8.754

Jach, G., M. Pesch, K. Richter, S. Frings, and J.F. Uhrig. 2006. An improved mRFP1 adds red to bimolecular fluorescence complementation. *Nat. Methods.* 3:597–600. http://dx.doi.org/10.1038/nmeth901

Jeon, J.H., S.S. Paik, M.H. Chun, U. Oh, and I.B. Kim. 2013. Presynaptic localization and possible function of calcium-activated chloride channel anoctamin 1 in the mammalian retina. *PLoS ONE.* 8:e67989. http://dx.doi.org/10.1371/journal.pone.0067989

Jung, J., J.H. Nam, H.W. Park, U. Oh, J.H. Yoon, and M.G. Lee. 2013. Dynamic modulation of ANO1/TMEM16A HCO3(-) permeability by Ca2+/calmodulin. *Proc. Natl. Acad. Sci. USA.* 110:360–365. http://dx.doi.org/10.1073/pnas.1211594110

Kaneko, H., I. Putzier, S. Frings, U.B. Kaupp, and T. Gensch. 2004. Chloride accumulation in mammalian olfactory sensory neurons. *J. Neurosci.* 24:7931–7938. http://dx.doi.org/10.1523/JNEUROSCI.2115-04.2004

Kaneko, H., F. Möhrlen, and S. Frings. 2006. Calmodulin contributes to gating control in olfactory calcium-activated chloride channels. *J. Gen. Physiol.* 127:737–748. http://dx.doi.org/10.1085/jgp.200609497

Kasri, N.N., K. Török, A. Galione, C. Garnham, G. Callewaert, L. Missiaen, J.B. Parys, and H. De Smedt. 2006. Endogenously bound calmodulin is essential for the function of the inositol 1,4,5-trisphosphate receptor. *J. Biol. Chem.* 281:8332–8338. http://dx.doi.org/10.1074/jbc.M510971200

Kim, S., L. Ma, and C.R. Yu. 2011. Requirement of calcium-activated chloride channels in the activation of mouse vomeronasal neurons. *Nat Commun.* 2:365. http://dx.doi.org/10.1038/ncomms1368

Kunzelmann, K., Y. Tian, J.R. Martins, D. Faria, P. Kongsuphol, J. Ousingsawat, F. Thevenod, E. Roussa, J. Rock, and R. Schreiber. 2011. Anoctamins. *Pflugers Arch.* 462:195–208. http://dx.doi.org/10.1007/s00424-011-0975-9

Kunzelmann, K., B. Nilius, G. Owsianik, R. Schreiber, J. Ousingsawat, L. Sirianant, P. Wanitchakool, E.M. Bevers, and J.W. Heemskerk. 2013. Molecular functions of anoctamin 6 (TMEM16F): a chloride channel, cation channel, or phospholipid scramblase? *Pflugers Arch.* In press. http://dx.doi.org/10.1007/s00424-013-1305-1

Kursula, P., and V. Majava. 2007. A structural insight into lead neurotoxicity and calmodulin activation by heavy metals. *Acta Crystallogr. Sect. F Struct. Biol. Cryst. Commun.* 63:653–656. http://dx.doi.org/10.1107/S1744309107034525

Lee, A., S.T. Wong, D. Gallagher, B. Li, D.R. Storm, T. Scheuer, and W.A. Catterall. 1999. Ca2+/calmodulin binds to and modulates P/Q-type calcium channels. *Nature.* 399:155–159. http://dx.doi.org/10.1038/20194

Li, F., S. Ponissery-Saidu, K.K. Yee, H. Wang, M.L. Chen, N. Iguchi, G. Zhang, P. Jiang, J. Reisert, and L. Huang. 2013. Heterotrimeric G protein subunit Gγ13 is critical to olfaction. *J. Neurosci.* 33:7975–7984. http://dx.doi.org/10.1523/JNEUROSCI.5563-12.2013

Lindemann, B. 2001. Predicted profiles of ion concentrations in olfactory cilia in the steady state. *Biophys. J.* 80:1712–1721. http://dx.doi.org/10.1016/S0006-3495(01)76142-5

Liu, B., J.E. Linley, X. Du, X. Zhang, L. Ooi, H. Zhang, and N. Gamper. 2010. The acute nociceptive signals induced by bradykinin in rat sensory neurons are mediated by inhibition of M-type K+ channels and activation of Ca2+-activated Cl^- channels. *J. Clin. Invest.* 120:1240–1252. http://dx.doi.org/10.1172/JCI41084

Martins, J.R., D. Faria, P. Kongsuphol, B. Reisch, R. Schreiber, and K. Kunzelmann. 2011. Anoctamin 6 is an essential component of the outwardly rectifying chloride channel. *Proc. Natl. Acad. Sci. USA.* 108:18168–18172. http://dx.doi.org/10.1073/pnas.1108094108

Mercer, A.J., K. Rabl, G.E. Riccardi, N.C. Brecha, S.L. Stella Jr., and W.B. Thoreson. 2011. Location of release sites and calcium-activated chloride channels relative to calcium channels at the photoreceptor ribbon synapse. *J. Neurophysiol.* 105:321–335. http://dx.doi.org/10.1152/jn.00332.2010

Mori, M.X., M.G. Erickson, and D.T. Yue. 2004. Functional stoichiometry and local enrichment of calmodulin interacting with Ca2+ channels. *Science.* 304:432–435. http://dx.doi.org/10.1126/science.1093490

Owenius, R., M. Osterlund, M. Lindgren, M. Svensson, O.H. Olsen, E. Persson, P.O. Freskgård, and U. Carlsson. 1999. Properties of spin and fluorescent labels at a receptor-ligand interface. *Biophys. J.* 77:2237–2250. http://dx.doi.org/10.1016/S0006-3495(99)77064-5

Patton, C., S. Thompson, and D. Epel. 2004. Some precautions in using chelators to buffer metals in biological solutions. *Cell Calcium.* 35:427–431. http://dx.doi.org/10.1016/j.ceca.2003.10.006

Payne, J.A., C. Rivera, J. Voipio, and K. Kaila. 2003. Cation-chloride co-transporters in neuronal communication, development and trauma. *Trends Neurosci.* 26:199–206. http://dx.doi.org/10.1016/S0166-2236(03)00068-7

Peersen, O.B., T.S. Madsen, and J.J. Falke. 1997. Intermolecular tuning of calmodulin by target peptides and proteins: differential effects on Ca2+ binding and implications for kinase activation. *Protein Sci.* 6:794–807. http://dx.doi.org/10.1002/pro.5560060406

Peterson, B.Z., C.D. DeMaria, J.P. Adelman, and D.T. Yue. 1999. Calmodulin is the Ca2+ sensor for Ca2+ -dependent inactivation of L-type calcium channels. *Neuron.* 22:549–558. http://dx.doi.org/10.1016/S0896-6273(00)80709-6

Pifferi, S., M. Dibattista, and A. Menini. 2009. TMEM16B induces chloride currents activated by calcium in mammalian cells. *Pflugers Arch.* 458:1023–1038. http://dx.doi.org/10.1007/s00424-009-0684-9

Pitt, G.S., R.D. Zühlke, A. Hudmon, H. Schulman, H. Reuter, and R.W. Tsien. 2001. Molecular basis of calmodulin tethering and Ca2+-dependent inactivation of L-type Ca2+ channels. *J. Biol. Chem.* 276:30794–30802. http://dx.doi.org/10.1074/jbc.M104959200

Ponissery Saidu, S., A.B. Stephan, A.K. Talaga, H. Zhao, and J. Reisert. 2013. Channel properties of the splicing isoforms of the olfactory calcium-activated chloride channel Anoctamin 2. *J. Gen. Physiol.* 141:691–703. http://dx.doi.org/10.1085/jgp.201210937

Qu, Z., and H.C. Hartzell. 2000. Anion permeation in Ca(2+)-activated Cl(-) channels. *J. Gen. Physiol.* 116:825–844. http://dx.doi.org/10.1085/jgp.116.6.825

Rasche, S., B. Toetter, J. Adler, A. Tschapek, J.F. Doerner, S. Kurtenbach, H. Hatt, H. Meyer, B. Warscheid, and E.M. Neuhaus. 2010. Tmem16b is specifically expressed in the cilia of olfactory sensory neurons. *Chem. Senses.* 35:239–245. http://dx.doi.org/10.1093/chemse/bjq007

Reisert, J., P.J. Bauer, K.W. Yau, and S. Frings. 2003. The Ca-activated Cl channel and its control in rat olfactory receptor neurons. *J. Gen. Physiol.* 122:349–363. http://dx.doi.org/10.1085/jgp.200308888

Reisert, J., J. Lai, K.W. Yau, and J. Bradley. 2005. Mechanism of the excitatory Cl- response in mouse olfactory receptor neurons. *Neuron.* 45:553–561. http://dx.doi.org/10.1016/j.neuron.2005.01.012

Schreiber, R., I. Uliyakina, P. Kongsuphol, R. Warth, M. Mirza, J.R. Martins, and K. Kunzelmann. 2010. Expression and function of epithelial anoctamins. *J. Biol. Chem.* 285:7838–7845. http://dx.doi.org/10.1074/jbc.M109.065367

Schroeder, B.C., T. Cheng, Y.N. Jan, and L.Y. Jan. 2008. Expression cloning of TMEM16A as a calcium-activated chloride channel subunit. *Cell.* 134:1019–1029. http://dx.doi.org/10.1016/j.cell.2008.09.003

Scudieri, P., E. Sondo, E. Caci, R. Ravazzolo, and L.J. Galietta. 2013. TMEM16A-TMEM16B chimaeras to investigate the structure-function relationship of calcium-activated chloride channels. *Biochem. J.* 452:443–455. http://dx.doi.org/10.1042/BJ20130348

Shen, Y., D. Yu, H. Hiel, P. Liao, D.T. Yue, P.A. Fuchs, and T.W. Soong. 2006. Alternative splicing of the Ca(v)1.3 channel IQ domain, a molecular switch for Ca2+-dependent inactivation within auditory hair cells. *J. Neurosci.* 26:10690–10699. http://dx.doi.org/10.1523/JNEUROSCI.2093-06.2006

Sheridan, J.T., E.N. Worthington, K.A. Yu, S.E. Gabriel, H.C. Hartzell, and R. Tarran. 2011. Characterization of the oligomeric structure of the Ca(2+)-activated Cl^- channel Ano1/TMEM16A. *J. Biol. Chem.* 286:1381–1388. http://dx.doi.org/10.1074/jbc.M110.174847

Shimizu, T., T. Iehara, K. Sato, T. Fujii, H. Sakai, and Y. Okada. 2013. TMEM16F is a component of a Ca2+-activated Cl^- channel but not a volume-sensitive outwardly rectifying Cl^- channel. *Am. J. Physiol. Cell Physiol.* 304:C748–C759. http://dx.doi.org/10.1152/ajpcell.00228.2012

Sigworth, F.J. 1980. The variance of sodium current fluctuations at the node of Ranvier. *J. Physiol.* 307:97–129.

Stephan, A.B., E.Y. Shum, S. Hirsh, K.D. Cygnar, J. Reisert, and H. Zhao. 2009. ANO2 is the cilial calcium-activated chloride channel that may mediate olfactory amplification. *Proc. Natl. Acad. Sci. USA.* 106:11776–11781. http://dx.doi.org/10.1073/pnas.0903304106

Stephan, A.B., S. Tobochnik, M. Dibattista, C.M. Wall, J. Reisert, and H. Zhao. 2011. The Na(+)/Ca(2+) exchanger NCKX4 governs termination and adaptation of the mammalian olfactory response. *Nat. Neurosci.* 15:131–137. http://dx.doi.org/10.1038/nn.2943

Stöhr, H., J.B. Heisig, P.M. Benz, S. Schöberl, V.M. Milenkovic, O. Strauss, W.M. Aartsen, J. Wijnholds, B.H.F. Weber, and H.L. Schulz. 2009. TMEM16B, a novel protein with calcium-dependent chloride channel activity, associates with a presynaptic protein complex in photoreceptor terminals. *J. Neurosci.* 29:6809–6818. http://dx.doi.org/10.1523/JNEUROSCI.5546-08.2009

Stroffekova, K. 2008. Ca2+/CaM-dependent inactivation of the skeletal muscle L-type Ca2+ channel (Cav1.1). *Pflugers Arch.* 455:873–884. http://dx.doi.org/10.1007/s00424-007-0344-x

Szteyn, K., E. Schmid, M.K. Nurbaeva, W. Yang, P. Münzer, K. Kunzelmann, F. Lang, and E. Shumilina. 2012. Expression and functional significance of the Ca(2+)-activated Cl(-) channel ANO6 in dendritic cells. *Cell. Physiol. Biochem.* 30:1319–1332. http://dx.doi.org/10.1159/000343321

Thoreson, W.B., R. Nitzan, and R.F. Miller. 2000. Chloride efflux inhibits single calcium channel open probability in vertebrate photoreceptors: chloride imaging and cell-attached patch-clamp recordings. *Vis. Neurosci.* 17:197–206. http://dx.doi.org/10.1017/S0952523800172025

Thoreson, W.B., S.L. Stella Jr., E.I. Bryson, J. Clements, and P. Witkovsky. 2002. D2-like dopamine receptors promote interactions between calcium and chloride channels that diminish rod synaptic transfer in the salamander retina. *Vis. Neurosci.* 19:235–247. http://dx.doi.org/10.1017/S0952523802192017

Thoreson, W.B., E.J. Bryson, and K. Rabl. 2003. Reciprocal interactions between calcium and chloride in rod photoreceptors. *J. Neurophysiol.* 90:1747–1753. http://dx.doi.org/10.1152/jn.00932.2002

Tian, Y., P. Kongsuphol, M. Hug, J. Ousingsawat, R. Witzgall, R. Schreiber, and K. Kunzelmann. 2011. Calmodulin-dependent activation of the epithelial calcium-dependent chloride channel TMEM16A. *FASEB J.* 25:1058–1068. http://dx.doi.org/10.1096/fj.10-166884

Tian, Y., R. Schreiber, and K. Kunzelmann. 2012. Anoctamins are a family of Ca2+-activated Cl^- channels. *J. Cell Sci.* 125:4991–4998. http://dx.doi.org/10.1242/jcs.109553

Tien, J., H.Y. Lee, D.L. Minor Jr., Y.N. Jan, and L.Y. Jan. 2013. Identification of a dimerization domain in the TMEM16A calcium-activated chloride channel (CaCC). *Proc. Natl. Acad. Sci. USA.* 110:6352–6357. http://dx.doi.org/10.1073/pnas.1303672110

Tran, T.T., K. Tobiume, C. Hirono, S. Fujimoto, K. Mizuta, K. Kubozono, H. Inoue, M. Itakura, M. Sugita, and N. Kamata. 2013. TMEM16E (GDD1) exhibits protein instability and distinct characteristics in chloride channel/pore forming ability. *J. Cell. Physiol.* In press. http://dx.doi.org/10.1002/jcp.24431

Trudeau, M.C., and W.N. Zagotta. 2004. Dynamics of Ca2+-calmodulin-dependent inhibition of rod cyclic nucleotide-gated channels measured by patch-clamp fluorometry. *J. Gen. Physiol.* 124:211–223. http://dx.doi.org/10.1085/jgp.200409101

Ungerer, N., N. Mücke, J. Broecker, S. Keller, S. Frings, and F. Möhrlen. 2011. Distinct binding properties distinguish LQ-type calmodulin-binding domains in cyclic nucleotide-gated channels. *Biochemistry.* 50:3221–3228. http://dx.doi.org/10.1021/bi200115m

Whelan, S., and N. Goldman. 2001. A general empirical model of protein evolution derived from multiple protein families using a maximum-likelihood approach. *Mol. Biol. Evol.* 18:691–699. http://dx.doi.org/10.1093/oxfordjournals.molbev.a003851

Williams, D.A., and F.S. Fay. 1990. Intracellular calibration of the fluorescent calcium indicator Fura-2. *Cell Calcium.* 11:75–83. http://dx.doi.org/10.1016/0143-4160(90)90061-X

Xia, X.M., B. Fakler, A. Rivard, G. Wayman, T. Johnson-Pais, J.E. Keen, T. Ishii, B. Hirschberg, C.T. Bond, S. Lutsenko, et al. 1998. Mechanism of calcium gating in small-conductance calcium-activated potassium channels. *Nature.* 395:503–507. http://dx.doi.org/10.1038/26758

Xiao, Q., K. Yu, P. Perez-Cornejo, Y. Cui, J. Arreola, and H.C. Hartzell. 2011. Voltage- and calcium-dependent gating of TMEM16A/Ano1 chloride channels are physically coupled by the first intracellular loop. *Proc. Natl. Acad. Sci. USA.* 108:8891–8896. http://dx.doi.org/10.1073/pnas.1102147108

Yamazaki, J., T. Urushidani, and T. Nagao. 1996. Barium activates rat cerebellar nitric oxide synthase. *Jpn. J. Pharmacol.* 70:351–354. http://dx.doi.org/10.1254/jjp.70.351

Yang, C., and R.J. Delay. 2010. Calcium-activated chloride current amplifies the response to urine in mouse vomeronasal sensory neurons. *J. Gen. Physiol.* 135:3–13. http://dx.doi.org/10.1085/jgp.200910265

Yang, P.S., B.A. Alseikhan, H. Hiel, L. Grant, M.X. Mori, W. Yang, P.A. Fuchs, and D.T. Yue. 2006. Switching of Ca2+-dependent inactivation of Ca(v)1.3 channels by calcium binding proteins of auditory hair cells. *J. Neurosci.* 26:10677–10689. http://dx.doi.org/10.1523/JNEUROSCI.3236-06.2006

Yang, Y.D., H.W. Cho, J.Y. Koo, M.H. Tak, Y.Y. Cho, W.S. Shim, S.P. Park, J. Lee, B. Lee, B.M. Kim, et al. 2008. TMEM16A confers receptor-activated calcium-dependent chloride conductance. *Nature.* 455:1210–1215. http://dx.doi.org/10.1038/nature07313

Yang, H., A. Kim, T. David, D. Palmer, T. Jin, J. Tien, F. Huang, T. Cheng, S.R. Coughlin, Y.N. Jan, and L.Y. Jan. 2012. TMEM16F forms a Ca2+-activated cation channel required for lipid scrambling in platelets during blood coagulation. *Cell.* 151:111–122. http://dx.doi.org/10.1016/j.cell.2012.07.036

Yap, K.L., J. Kim, K. Truong, M. Sherman, T. Yuan, and M. Ikura. 2000. Calmodulin target database. *J. Struct. Funct. Genomics.* 1:8–14. http://dx.doi.org/10.1023/A:1011320027914

Yu, K., C. Duran, Z. Qu, Y.Y. Cui, and H.C. Hartzell. 2012. Explaining calcium-dependent gating of anoctamin-1 chloride channels requires a revised topology. *Circ. Res.* 110:990–999. http://dx.doi.org/10.1161/CIRCRESAHA.112.264440

Zühlke, R.D., G.S. Pitt, K. Deisseroth, R.W. Tsien, and H. Reuter. 1999. Calmodulin supports both inactivation and facilitation of L-type calcium channels. *Nature.* 399:159–162. http://dx.doi.org/10.1038/20200